Master of Science Thesis

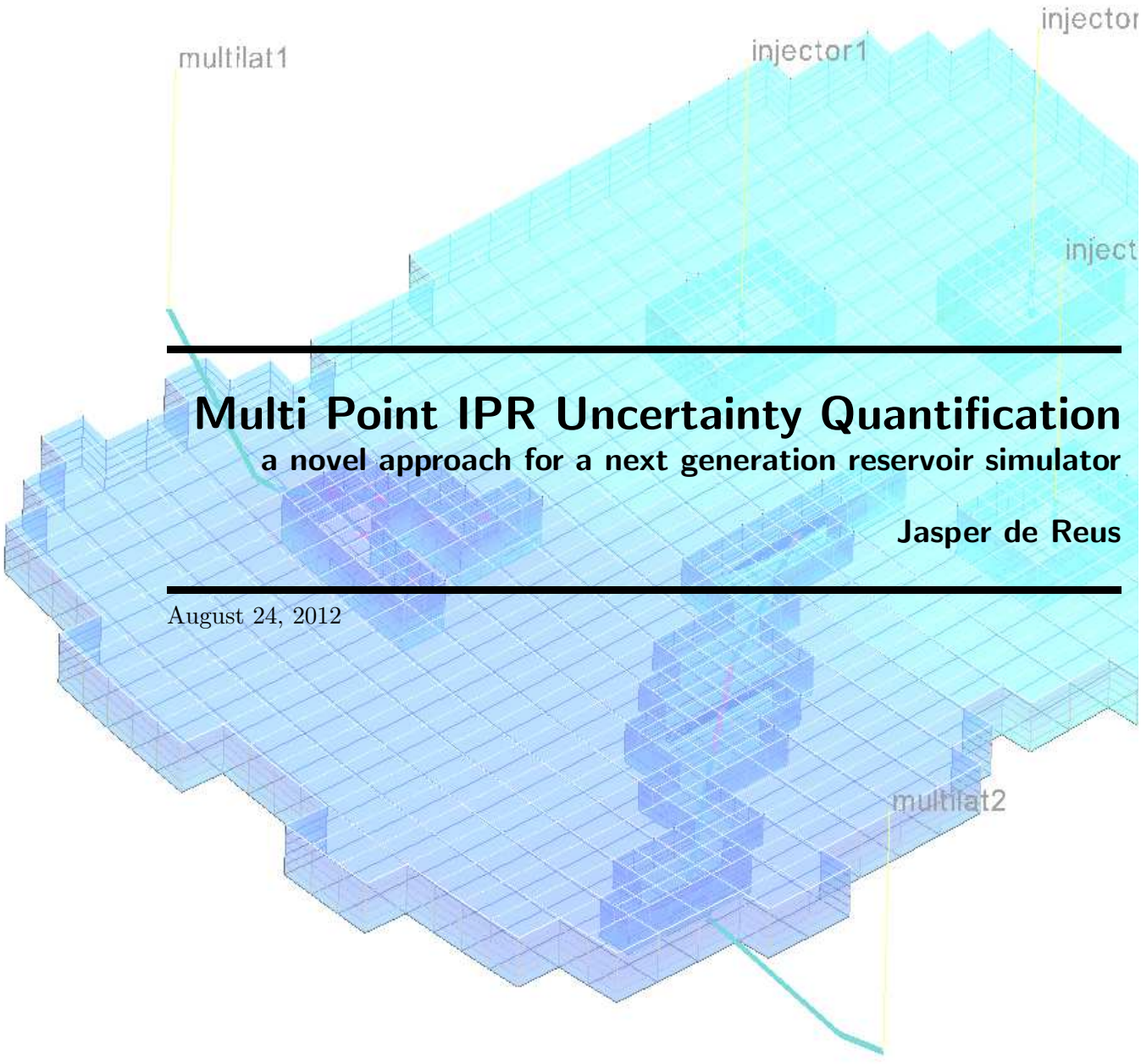

Multi Point IPR Uncertainty Quantification

a novel approach for a next generation reservoir simulator

Jasper de Reus

August 24, 2012

Shell Global Solutions
Dynamic Modeling

Delft University of Technology
Faculty of Aerospace Engineering

Multi Point IPR Uncertainty Quantification

a novel approach for a next generation reservoir simulator

Master of Science Thesis

For obtaining the degree of Master of Science in Aerospace Engineering at Delft University of Technology

Jasper de Reus

August 24, 2012

Shell Global Solutions · Delft University of Technology

Delft University of Technology

Delft University Of Technology
Department Of
Aerodynamics

The undersigned hereby certify that they have read and recommend to the Faculty of Aerospace Engineering for acceptance a thesis entitled **"Multi Point IPR Uncertainty Quantification"** by **Jasper de Reus** in partial fulfillment of the requirements for the degree of **Master of Science**.

Dated: August 24, 2012

Head of department: _____
Prof.dr.ir. H. Bijl

Supervisor: _____
Dr. R.P. Dwight

Reader: _____
Dr. D. Zwarts

Reader: _____
Ir. W.N. Edeling

Abstract

It is investigated if a Multi Point Inflow Performance Relationship (MIPR) using Uncertainty Quantification (UQ) can lead to a step change in completion design. The MIPR model consists of several Kuchuk IPR models coupled with a wellbore network, and is verified against a discretized model. It is found that the assumption of artificial no-flow boundaries for this model is limiting, which leads to an overprediction of the distributed productivity index. A calibration using Markov Chain Monte Carlo (MCMC) is preformed, which incorporates both epistemic and aleatory model parameters. In addition, a more efficient 'partitioned MCMC' is investigated, which shows promising results. The UQ MIPR model can predict the change in productivity index due to a uniform completion skin profile, and can give an indication of results for a non-uniform change in completion skin. In conjunction with a discretized model, a MIPR model can lead to a step change in completion by providing information to a production technologists earlier on in field development.

Acknowledgments

I still remember the excitement of the VSV introduction weekend for first year students as if it were yesterday. During the six year journey that followed, the excitement kept on growing; first with the successful record attempt of the Stratos rocket in Sweden and next with being able to contribute to the design of a novel plane during an internship in South Africa. In the last year of my study I have had the fantastic opportunity to write my thesis at the dynamic reservoir modeling group at Shell. During this adventure into the unfamiliar fields of reservoir engineering, uncertainty quantification and information technology, I have had a tremendous amount of support from supervisors, colleagues and friends that I would like to acknowledge.

I would like to thank my Shell supervisor John Hudson allowing me to undertake this thesis project under his guidance. Despite the eight hour time difference between us, his knowledge, friendliness and patience have made this a very rewarding year for me. I am also very grateful for the support of Richard Dwight, my supervisor at the TU Delft. Especially his early Friday morning meetings addressing uncertainty quantification have been very helpful and informative. I would like to thank Hester Bijl for her excellent coaching on a topic that is not directly related to aerodynamics. Furthermore, I am grateful for the assistance of all my team members and managers at Shell. Many other colleagues have contributed to this project, including Roelof Darling, Murat Kerem and Dirk Zwarts.

My journey into aerospace engineering has been made possible thanks to the encouragement of my parents, to whom I owe a lot. Finally, I would like to thank my girlfriend, Sophia, for all her care during this adventure.

Contents

Abstract v

Acknowledgments vii

List of Figures xiii

List of Tables xv

Nomenclature xvii

I Problem Definition 1

Introduction 3

1 Petroleum Engineering 5

1.1 Petroleum Engineering Concepts 5

1.1.1 Reservoir 5

1.1.2 Well 6

1.1.3 Fluid Flow 6

1.1.4 Subsurface Data Acquisition 8

1.2 Inflow Performance Relationship 9

1.2.1 Introduction to IPR 9

1.2.2 Kuchuk IPR 11

1.2.3 Discretized Model 15

1.2.4 Potential for an Intermediate Fidelity IPR 16

2 Uncertainty Quantification **17**
2.1 UQ Concepts . . . 17
2.2 Bayesian Inference . . . 18
2.3 Monte Carlo . . . 18
2.4 Markov Chain Monte Carlo . . . 19
2.5 Application of UQ in Petroleum Engineering . . . 19

3 Problem Definition and Approach **21**
3.1 Thesis Question Relevance . . . 21
3.2 MIPR UQ Approach . . . 22

II MIPR Uncertainty Quantification and Calibration **23**

4 MIPR Model **25**
4.1 Introduction to MIPR . . . 25
4.2 MIPR Model Description . . . 25
4.2.1 Well Network Models . . . 27
4.2.2 Solution Process . . . 28
4.3 MIPR Assumptions . . . 29

5 MIPR Verification **31**
5.1 Model Gridding Verification . . . 31
5.1.1 Discertized Model Grid . . . 31
5.1.2 MIPR Zones . . . 32
5.2 Homogeneous Drainage Area Verification . . . 34
5.2.1 Individual Parameter Verification . . . 34
5.2.2 Latin Hypercube Sampling . . . 36
5.3 Heterogeneous Drainage Area Verification . . . 38
5.4 Conclusion . . . 40

6 MIPR Calibration **43**
6.1 Calibration Approach . . . 43
6.1.1 Model and Data . . . 43
6.1.2 Parameter Selection . . . 43
6.1.3 Sensitivity Study . . . 45
6.1.4 Calibration Approach . . . 45
6.2 Calibration Theory Application . . . 46
6.2.1 Deterministic Calibration . . . 46
6.2.2 MIPR Bayesian Inference . . . 47
6.3 Results Bayesian Inference . . . 50
6.3.1 Calibration Method Verification . . . 50
6.3.2 Calibration Results with Aleatory Uncertainty . . . 51
6.4 Analysis of pMCMC . . . 53
6.4.1 Step Acceptance Comparison Between MCMC and pMCMC . . . 53
6.4.2 Simple pMCMC Experiment . . . 56
6.5 Conclusion . . . 57

7 MIPR Prediction **59**
7.1 Prediction for a Homogeneous Completion Skin Profile 59
7.2 Prediction for a Heterogeneous Completion Skin Profile 59
7.3 Conclusion 61

8 Conclusions and Recommendations **63**
8.1 Conclusions 63
8.2 Recommendations 64
8.2.1 Model Recommendations 64
8.2.2 Calibration Recommendations 65

References **67**

A Theory **71**
A.1 Black Oil Reservoir Simulation 71
A.2 Peaceman Inflow Model 72
A.3 Newton–Rhapson Linearization 73

B Tables **75**

List of Figures

1.1 Diagram of a reservoir 6
1.2 Well completion types 7
1.3 VLP IPR curve 10
1.4 Kuchuk domain 12

4.1 MIPR illustration 26
4.2 MIPR wellbore network topology 26

5.1 Discretized model grid convergence for PI 33
5.2 Discretized model grid convergence for PI_L 34
5.3 MIPR zone convergence for PI 35
5.4 MIPR zone convergence for PI_L 36
5.5 PI verification for individual parameters 37
5.6 PI Kuchuk and MIRP percentage offset from a discretized model 38
5.7 PI_L for MIPR and discretized model 40

6.1 Sensitivity study for zone four 46
6.2 Sensitivity study for zone six 47
6.3 s_β with measurement uncertainty only 51
6.4 Predicted PI_L with measurement uncertainty only 52
6.5 s_β with full uncertainty 53
6.6 Predicted PI_L for full uncertainty 54
6.7 s_β with full uncertainty calculated with pMCMC 55
6.8 Candidate steps 55

7.1 PI_L prediction for homogeneous skin with full uncertainty, 2984 samples. 60
7.2 PI_L prediction for heterogeneous skin with full uncertainty, 2984 samples. 61

List of Tables

4.1 Parameters in pipe model 28
4.2 Assumptions of the Kuchuk, MIPR and discretized model 29

5.1 Verification domain of MIPR and discretized model gridding investigation 32
5.2 Non-dimensional parameter definition 35
5.3 Verification sample space 37
5.4 Global heterogeneous verification domain of a MIPR and discretized model 39
5.5 Zonal heterogeneous verification domain of a MIPR and discretized model 39
5.6 Error in MIPR drawdown 39

6.1 Prior distributions for the global domain 44
6.2 Zonal prior permeability distributions 45
6.3 Posterior b for the aleatory and epistemic case 57

B.1 PUNQ oil table 75
B.2 PUNQ gas table 76
B.3 Additional oil parameters 76
B.4 Unit conversion factors 77

Nomenclature

Latin Symbols

A	Area	$[m^2]$
B	Volume formation factor	$[m^3/std\ m^3]$
B_g	Gas volume formation factor	$[m^3/std\ m^3]$
B_o	Oil volume formation factor	$[m^3/std\ m^3]$
c_f	Fluid compressibility coefficient	$[1/Pa]$
c_t	Total compressibility coefficient	$[1/Pa]$
c_o	Oil compressibility coefficient	$[1/Pa]$
c_R	Rock compressibility coefficient	$[1/Pa]$
c_{vo}	Oil viscosibility coefficient	$[1/Pa]$
d	Pipe diameter	$[m]$
f_{tp}	Two phase friction factor	$[-]$
g	Gravitational acceleration	$[m/s^2]$
G_m	Mixture mass flux rate	$[kg/sm^2]$
H_L	Liquid holdup	$[-]$
J	Productivity Index	$[std\ m^3/Pa\ s]$
K	Markov chain transition matrix	$[-]$
k	Permeability	$[m^2]$
L_{wh}	Completion half length	$[m]$
L_x	Drainage area length in x direction	$[m]$
L_y	Drainage area length in y direction	$[m]$
L_z	Drainage area length in z direction	$[m]$

m_g	Gas molecular mass	$[kg/mol]$
m_o	Oil molecular mass	$[kg/mol]$
N	Number of stochastic samples	$[-]$
p	Pressure	$[Pa]$
p_r	Average reservoir pressure	$[Pa]$
p_{wf}	Bottom hole flowing well pressure	$[Pa]$
q	Mass flow rate	$[kg/s]$
q_v	Volumetric flow rate	$[std\ m^3/s]$
r_e	Radial length to edge of reservoir	$[m]$
r_{eq}	Equivalent radius	$[m]$
Rs	Solution gas oil ratio	$[std\ m^3/std\ m^3]$
r_w	Wellbore radius	$[m]$
r'_w	Scaled wellbore radius	$[m]$
S	Saturation	$[-]$
s	Skin	$[-]$
S_{zd}	Vertical skin	$[-]$
t	Time	$[s]$
U	Random sample	$[-]$
u	Darcy velocity	$[m/s]$
V_b	Bulk volume	$[m^3]$
V_p	Non-isolated pore volume	$[m^3]$
w	Mass flow rate	$[kg/s]$
w_f	Friction losses	$[m^2/s^2]$
x	Axial coordinate	$[m]$
x_w	Position of center of well in x direction	$[m]$
y_w	Position of center of well in y direction	$[m]$
Z	Coordinate along pipe	$[m]$
z_w	Position of center of well in z direction	$[m]$

Greek Symbols

α	Aleatory set of domain and boundary parameters	$[-]$
β	Set of epistemic parameters	$[-]$
γ	Intermediate Kuchuk variable	$[1/m]$
ϵ	Measurement error	$[std\ m^3/Pas]$
θ	Pipe inclination angle from horizontal	$[rad]$
μ	Viscosity	$[Pas]$
ν_m	Mixture velocity	$[m/s]$

ν_{sg}	Superficial gas velocity	$[m/s]$
ν_{sl}	Superficial liquid velocity	$[m/s]$
ξ	Intermediate Kuchuk variable	$[-]$
π	Distribution of Markov chain	$[-]$
ρ	Density	$[kg/m^3]$
ρ_L	Density of the liquid phase	$[kg/m^3]$
ρ_{tp}	Two phase mixture density	$[kg/m^3]$
σ	Standard deviation	$[-]$
Φ	MCMC state	$[-]$
ϕ	Porosity (effective)	$[-]$
Ψ	Anisotropy	$[-]$

Subscripts

$_D$	Data
$_d$	Dimensionless
$_g$	Gas phase
$_o$	Oil phase
$_r$	Relative
$_w$	Water phase

Abbreviations

DM	Discretized Model
IPR	Inflow Performance Relationship
MCMC	Markov Chain Monte Carlo
MIPR	Multi Point IPR
PI	Productivity Index
VLP	Vertical Lift Performance

Other Symbols

Δ	Discretized unit
$\mathcal{L}_m$	Linear differential operator
p	Probability operator
∇	Gradient operator

Part I

Problem Definition

Introduction

The world's population of seven billion people can only be sustained if there is a plentiful supply of energy. Today over 84% of this energy is drawn from fossil fuels, and even by 2035 it is estimated that only 26% of the world's energy will come from renewable sources Tanaka [2010]. However, over past decades, the amount of discovered oil and gas has been steadily declining Helman [2011]. It is therefore essential that current reservoirs are developed as efficiently as possible, and it is here where this thesis aims to make an impact. The research, which has been performed at Shell, focusses on the following thesis question: 'Can a horizontal Multi Point IPR model incorporating Uncertainty Quantification lead to a step change in completion design?'

Part I covers the concepts of IPR equations and Uncertainty Quantification in Chapters 1 and 2, before the problem definition and approach is elaborated upon in Chapter 3. Part II covers the research performed to answer the thesis question, with an Multi Point IPR description, verification and calibration in Chapter 4, 5 and 6, respectively. Chapter 7 addresses the prediction of the calibrated Multi Point IPR.

Chapter 1

Petroleum Engineering

Petroleum engineering is a collection of disciplines involved in the extraction of hydrocarbons from the Earth's crust. This chapter serves as an introduction to the concepts and terminology required to understand the context of the thesis question. The governing partial differential equations of reservoir flow are stated, from which simplified Inflow Performance Relationships are derived. These models are subsequently verified and calibrated in Chapter 5 and 6.

1.1 Petroleum Engineering Concepts

Three key concepts in petroleum engineering are the reservoir, well, and reservoir fluids, described in Section 1.1.1 through 1.1.3. In Section 1.1.4, subsurface measurement techniques are introduced.

1.1.1 Reservoir

A petroleum reservoir is a porous domain of rock containing hydrocarbons. Reservoirs form when ancient organic material becomes trapped under impermeable cap rock. Typically, a reservoir consists of an aquifer, oil layer and, in many cases, a gas cap. An illustration of a reservoir is depicted in Figure 1.1.

The water and hydrocarbons are contained in rock pores. The (effective) porosity, ϕ, is a measure of the connected empty space in a rock, and is described by (1.1)

$$\phi = \frac{V_p}{V_b}. \tag{1.1}$$

Here V_p is the non-isolated pore volume and V_b is the bulk volume of the rock. Typically the porosity range is from 0.1 to 0.3 Economides et al. [1993]. Permeability, k, characterizes the capacity of a rock to let fluids flow through these pores.

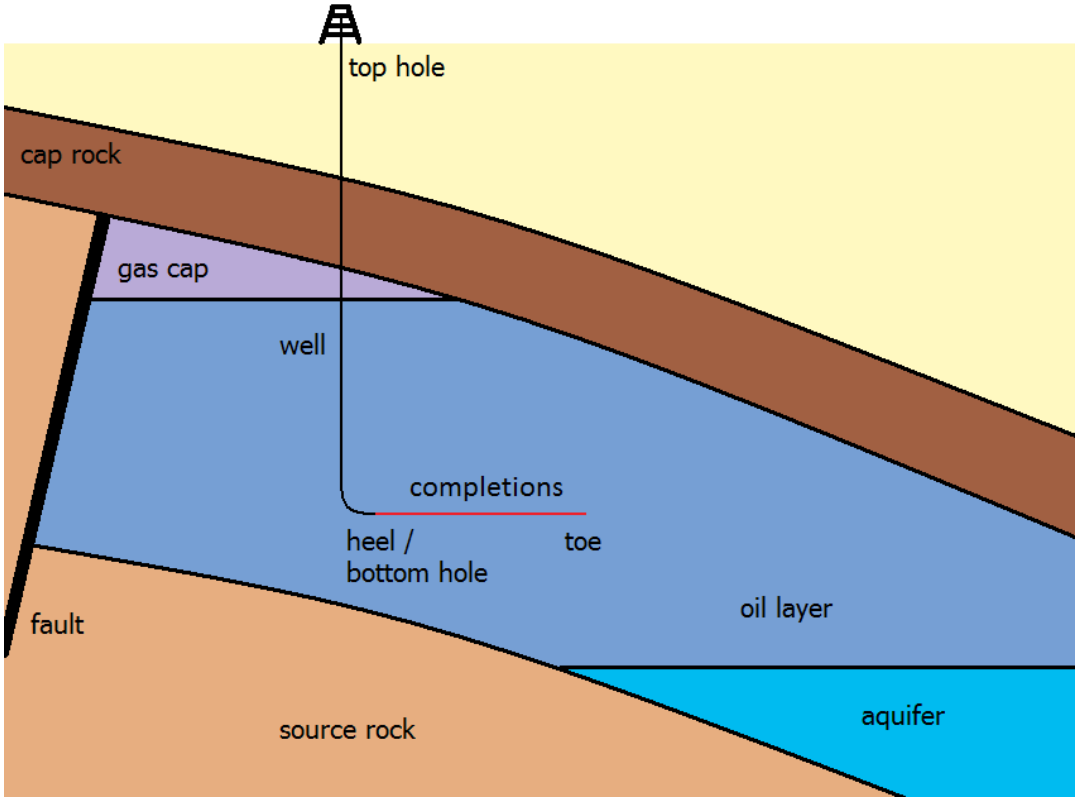

Figure 1.1: Diagram of a reservoir

The reservoir rock is inherently inhomogeneous. Not only are there features such as fractures and faults that can drastically increase permeability or form a no-flow boundary condition, the rock itself also has heterogeneity depending on its depositional structure. The permeability field can be anisotropic; the vertical permeability can be ten times smaller than that of horizontal directions Dake [1978].

1.1.2 Well

The connection between a reservoir and the surface is a well, the inside of which is called the wellbore. A horizontal well is illustrated in Figure 1.1. Completions are the interface between a well and a reservoir, these are designed to inhibit sand production while minimizing the pressure loss. A set of adjacent completions is called a perforation. The common types of completions are depicted in Figure 1.2. Production technologists are responsible for selecting the right completion strategy for a well.

1.1.3 Fluid Flow

The treatment of fluid flow through the reservoir differs from that in the wellbore.

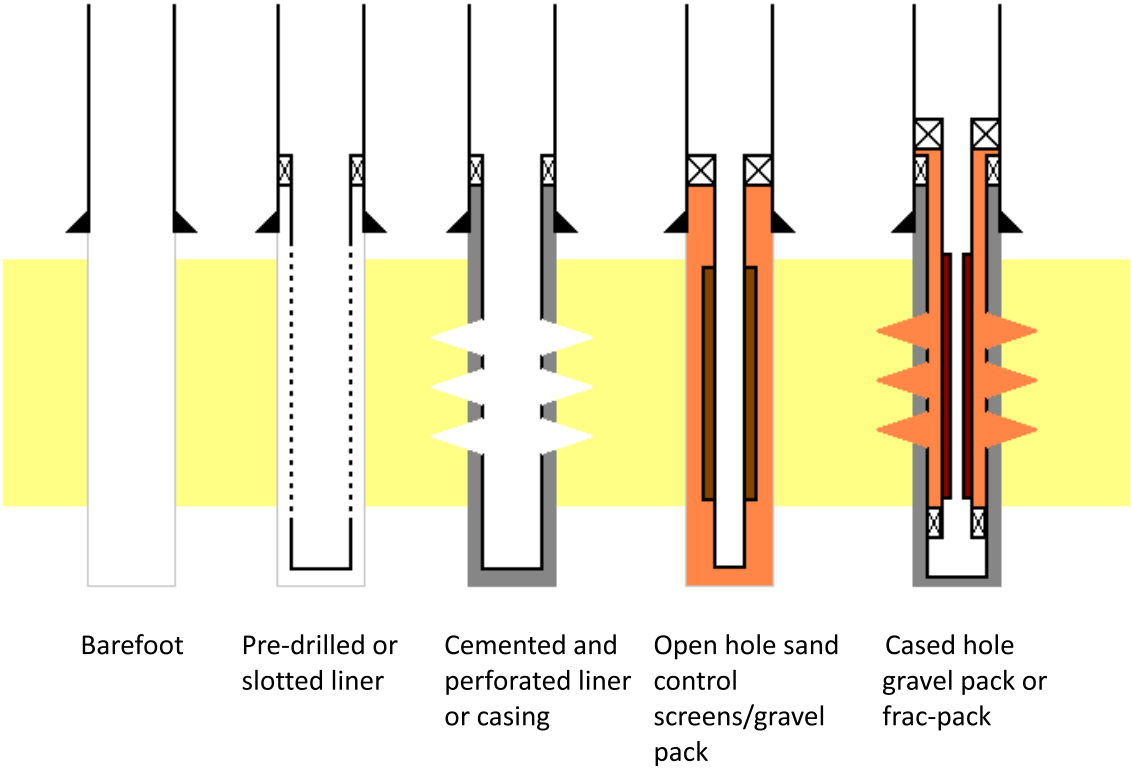

Figure 1.2: Well completion types Bellarby [2009]

Reservoir flow

A one-dimensional single phase fluid flow through porous media is governed by Darcy's law (1.2) Chen [2007]:

$$q_v = -\frac{kA}{\mu}\frac{\mathrm{d}p}{\mathrm{d}x_1}. \tag{1.2}$$

Here q_v is the volumetric flow rate over an area A. This flow rate is proportional to the pressure gradient. The symbol p denotes pressure, and μ the viscosity. Equation 1.2 above has been written for single phase flow. Multiphase flow requires the introduction of relative permeability's into Darcy's equations, as described in Appendix A.1.

The Darcy velocity is defined as

$$u = \frac{q_v}{A}. \tag{1.3}$$

For a three-dimensional flow in a horizontal reservoir, (1.2) and (1.3) can be written as

$$\mathbf{u} = \frac{-1}{\mu}\,\mathbf{k}(\nabla p). \tag{1.4}$$

In (1.4), $\mathbf{k}$ is the permeability tensor of size $[3 \times 3]$.

The mass conservation equation (1.5) is derived for a flow element by Chen [2007] as

$$\frac{\partial(\phi\rho)}{\partial t} = -\nabla \cdot (\rho\,\mathbf{u}) + q. \tag{1.5}$$

Here q represents the mass flow sources and sinks in the domain. Equation (1.5) states that the change in mass in a flow element over time can either be due to changes in a domain, namely the rock pore volume, density ρ, or the presence of a source or sink such as a well. Additionally, a chance in mass of the flow element can be due to a flux over the boundary of the element.

Combining (1.4) and (1.5) yields

$$\frac{\partial(\phi\rho)}{\partial t} = \nabla \cdot \left(\frac{\rho}{\mu}\,\mathbf{k}(\nabla p)\right) + q. \tag{1.6}$$

Equation (1.6) is the equation governing single phase compressible flow, including heterogeneous permeability and rock compressibility. A simplified form of (1.6) will be solved analytically in Section 1.2.2, which will form the basis of the IPR models to be investigated in this thesis.

Pipe flow

The physics of the reservoir flows described in the previous section differ from that of wellbore flows. There are numerous alternative models for wellbore flows, including empirical correlations and mechanistic models. Even when the reservoir flow is single phase, the wellbore pressures near the surface are often such that a gaseous component forms as well. Famous empirical correlations include those of Duns & Ros [1963], Orkiszewski [1967] and Hagedorn & Brown [1964]. Notable mechanistic models are those of Tailel & Dukler [1976], Ansari et al. [1994], Gomez et al. [2000] and Petalas & Aziz [2000]. For this thesis the model of Beggs & Brill [1973] is used, which consists of correlations for pipe flow with an inclination varying from horizontal to vertical. The equations of this model are addressed in Section 4.2.1.

1.1.4 Subsurface Data Acquisition

A number of parameters were introduced in the previous sections, such as permeability and porosity. There are a variety of methods to measure these parameters.

Seismic data, obtained using acoustic measurements at the surface, is the primary source of information for geologists to estimate the rock composition and extent of the reservoir.

This then forms the basis of what is called the static model. Seismic data typically has an areal resolution of 80 meters Fengshu et al. [2009]. In Nalonnil & Marion [2012], the typical vertical resolution of 15 meters has been reduced to one meter using cross well seismic imaging.

Several measurements can be obtained from a well to determine the near wellbore characteristics. A crude form of determining the geology of a reservoir is via mud logging, where rock cuttings are filtered out of the drilling fluid. Another measurement is coring, where a physical section of rock is extracted from the reservoir. Flow measurements and CAT scans are then used to measure permeability and porosity on a sub centimeter scale Serag et al. [2010].

Well logs made by lowering sensors down into the wellbore can determine the geology and fluids in the near wellbore region. These logs can include "multi-depth resistivity, gamma ray, neutron, density, dipole sonic, NMR, spectroscopy, resistivity imager and pressure/fluid samples." Scholtes & Saha [2008]. Data obtained from cores and well logs often show significant disagreement. Extensive literature has been written on reconciling this data; Adams [2005], Serag et al. [2010], Adams [2005]. Nevertheless, Fylling [2002] notes that the difference in independent evaluations of the same subsurface properties is on the order of ten percent. A table with parameter uncertainty is given in Maschio et al. [2009], where the permeability is found to have a standard deviation on the order of 10 $[mD]$.

Gouges that measure pressure, temperature and flow can be inserted permanently at the bottom hole. The latest technology for wellbore measurements is fiber optics. These measurement techniques are important for the MIPR calibration to be done in Chapter 6. In contrast with gouges, this can provide data at several stations along a perforation. Traditionally, fiber optic measurements have been restricted to temperature, but recent developments extend these to pressure and acoustic derived flow measurements Bond et al. [2004], K.Kragas et al. [2004]. Koelman et al. [2012] note that "when combined in a single downhole-deployable cable, these fiber optic sensing technologies promise to provide a much more complete picture of downhole conditions, thereby allowing operators to optimize workovers, completions, well lift and flow conformance." Fiber optics are not yet a wide-spread technology because of the challenging physics involved, large data volumes (1 TB/day), and high cost Koelman & Potters [2012].

1.2 Inflow Performance Relationship

1.2.1 Introduction to IPR

An Inflow Performance Relationship (IPR) gives a relation between the well flow and the difference between the bottom hole pressure p_{wf} and the average reservoir pressure p_r, called drawdown. It is a measure of what the reservoir can produce for a certain bottom hole pressure. The Vertical Lift Performance (VLP) is a curve determining how much flow a well can deliver to the surface, for a certain bottom hole pressure. Figure 1.3 illustrates the equilibrium operating point of the well-reservoir system, at the intersection of the IPR and VLP curves.

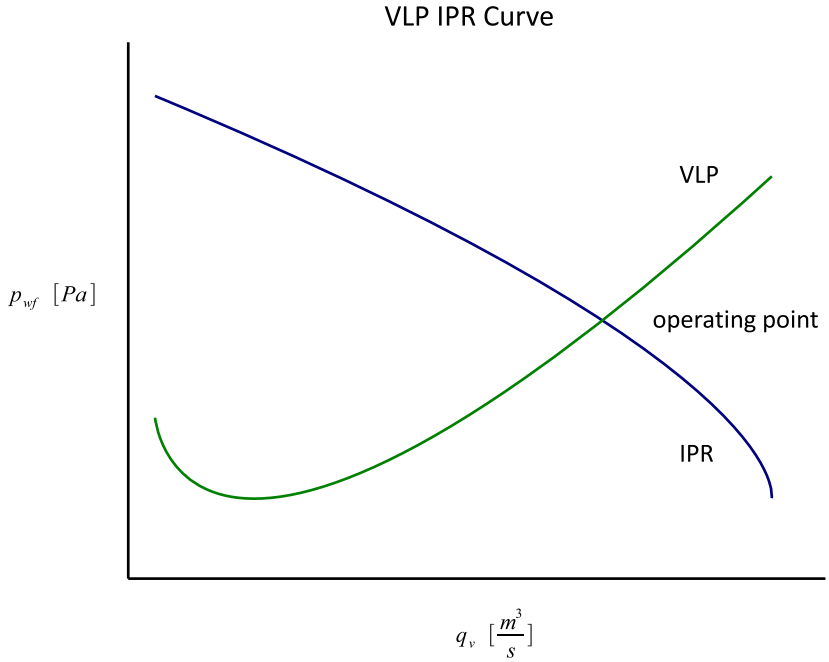

Figure 1.3: VLP IPR curve

For the region of laminar Darcy flow, which is the region of interest for this thesis, the IPR curve in Figure 1.3 has a linear form of (1.7)

$$q_v = J(p_{wb} - p_r). \tag{1.7}$$

The coefficient J is the Productivity Index (PI). One of the most basic IPR equations is that of Darcy IPR for a vertical well in the center of a cylindrical drainage area, written as (1.8)

$$q_v = \frac{kh(p_r - p_{wf})}{\mu B \left[\ln\left(\frac{r_e}{r_w} - 0.75 + s\right)\right]}. \tag{1.8}$$

Although this equation is not considered for this thesis, its basic form allows an easy interpretation of how subsurface parameters effect the PI. In (1.8) r_e is the radial length to the edge of the drainage area, r_w is the wellbore radius. B is the volume formation factor, which relates the change in volume of fluids from reservoir conditions to standard surface conditions.

The skin s is a composite modeling parameter representing a variety of different pressure drops or jumps used to approximate model inadequacies. For instance, drilling causes a reduction in permeability due to rock compression and drilling fluid infiltration into

the formation, hence the skin is increased. On the other hand, the insertion of a frack pack completion, or other forms of well stimulation, can be represented by a negative skin factor. An example of a model inadequacy correction is a 'reservoir skin', that can approximate the effect when the assumption of non-radial flow is violated. All model inaccuracy skins combined are called a 'calibration skin' in this thesis, which will be used in the calibration in Chapter 6.

Equation (1.8) holds for steady state flow, where the derivative of q with respect to time is constant. Pseudo steady state flow occurs when the effect of all the boundary conditions is felt at the wellbore. It can take several hours, or even weeks, before the transient effects of a change in bottom hole pressure become negligible Ahmed [2010]. Transient response interpretation is called well testing, and can be used for Bayesian inference of permeability and drainage area.

The main use of IPR models is optimizing perforation length and designing the well completion strategy. A large number of different IPR models exist, including models for horizontal wells. Early work in deriving analytical IPR models for horizontal wells has been performed by Giger et al. [1984], Karcher et al. [1986] and S. Joshi [1988]. The work of Karcher et al. [1986] focuses on a box shape drainage area where the completion is placed exactly in the center. In contrast, S. Joshi [1988] derived equations for a reservoir of infinite areal extent, with a completion placed at half the height of the reservoir. These models have been superseded by that of Goode & Kuchuk [1991], which allows considerably more freedom in the placement of the completion. For this reason, a Kuchuk IPR model is used for this thesis.

1.2.2 Kuchuk IPR

Goode & Kuchuk [1991] derived an analytical equation for a domain with no flow boundaries depicted in Figure 1.4. From here on, this model will be called the Kuchuk IPR model.

The equations in the domain of Figure 1.4 are derived from (1.6), rewritten in the form of (1.9)

$$\left(\phi\frac{\mathrm{d}\rho}{\mathrm{d}p}+\rho\frac{\mathrm{d}\phi}{\mathrm{d}p}\right)\frac{\partial p}{\partial t}=\nabla\cdot\left(\frac{\rho}{\mu}\mathbf{k}(\nabla p)\right)+q. \tag{1.9}$$

In (1.9), q represents sources or sinks, such as the presence of a well. If the assumption is made of slightly compressible flow, then according to Chen [2007], ρ can be approximated by a fluid compressibility coefficient c_f,

$$\rho\approx\rho^0(1+c_f(p-p^0)+O(c_f^2p^2)). \tag{1.10}$$

The rock compressibility coefficient c_R is given by (1.11)

$$c_R=\frac{1}{\phi}\frac{\mathrm{d}\phi}{\mathrm{d}p}. \tag{1.11}$$

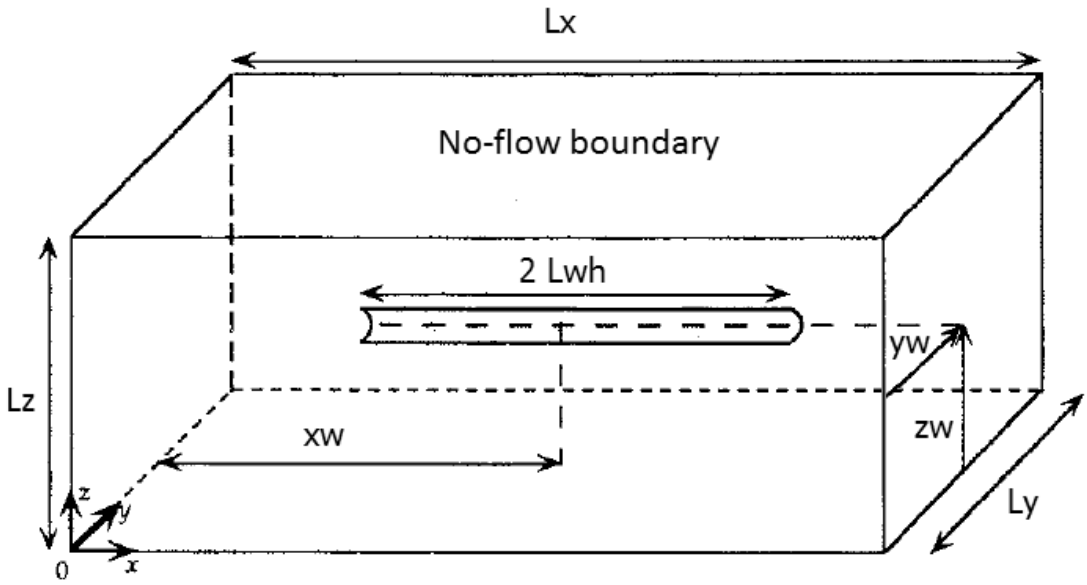

Figure 1.4: Kuchuk domain Goode & Kuchuk [1991]

Substituting (1.10) and (1.11) in (1.9) yields

$$\phi\rho c_t \frac{\partial p}{\partial t} = \nabla \cdot \left(\frac{\rho}{\mu} \mathbf{k}(\nabla p) \right) + q, \tag{1.12}$$

where the total compressibility c_t is defined as the fluid plus rock compressibility

$$c_t = c_f + \frac{\phi^0}{\phi} c_R. \tag{1.13}$$

Next, the dimensions of length can be scaled such that

$$\left\{ \begin{array}{c} \widetilde{x} \\ \widetilde{y} \\ \widetilde{z} \end{array} \right\} = \left\{ \begin{array}{c} x \\ y\sqrt{\frac{k_x}{k_y}} \\ z\sqrt{\frac{k_x}{k_z}} \end{array} \right\}. \tag{1.14}$$

An assumption can then be made that the permeability tensor is diagonal

$$\mathbf{k} = \text{diag}\{\text{kx, ky, kz}\}. \tag{1.15}$$

What this assumption implies is that the chosen axis system x, y and z must be the principal flow directions. Thus, the perforation must be parallel to one of the principal flow directions, with the other two orthogonal to it. This assumption is often not limiting for production technologists. Horizontal wells are often drilled such that the principal flow direction with the least resistance to flow is perpendicular to the well Dake [1978].

The anisotropy in (1.12) can then be eliminated, when a homogeneous medium is assumed. The source term q is removed, as it will be shown that the well can be treated as a boundary condition;

$$\frac{\phi\rho\mu c_t}{k_x}\frac{\partial p}{\partial t} = \widetilde{\nabla}\cdot\left(\rho(\widetilde{\nabla}p)\right). \tag{1.16}$$

Substituting (1.13) into (1.16),

$$\frac{\phi\rho c_t}{k_x}\frac{\partial p}{\partial t} = \widetilde{\Delta}p + \widetilde{\nabla}\cdot\left(c_f(p-p^0)(\widetilde{\nabla}p)\right). \tag{1.17}$$

Going beyond the assumption of slightly compressible flow, and assuming incompressibility altogether, the second term on the right hand side can be eliminated, leaving the Poisson equation that forms the basis for the model that is used for the remainder of this thesis:

$$\frac{\phi\rho c_t}{k_x}\frac{\partial p}{\partial t} = \widetilde{\Delta}p. \tag{1.18}$$

Equation (1.18) is then solved analytically by Goode & Kuchuk [1991], starting with

$$\frac{\partial p_d}{\partial t_d} = \frac{\partial^2 p_d}{\partial x_d^2} + \frac{\partial^2 p_d}{\partial y_d^2}, \tag{1.19}$$

for the domain surrounded by no flow boundary conditions as depicted in Figure 1.4. In (1.19), the dimensionless pressure p_d, time t_d, and horizontal dimensions x_d and y_d are defined as

$$p_d = 2\pi L_z\sqrt{k_x k_y}\frac{(p_r - p_{wf})}{q_v\mu}, \tag{1.20}$$

$$t_d = \frac{k_x t}{\phi\mu c_t L_x^2}, \tag{1.21}$$

$$x_d = \frac{x}{L_x}, \tag{1.22}$$

$$y_d = \sqrt{\frac{k_x}{k_y}}\frac{y}{L_x}. \tag{1.23}$$

Instead of an infinite conductivity boundary condition at the wellbore, the wellbore is represented as a strip boundary condition with a constant flux as in (1.24)

$$\lim_{y_d\to y_{wd}}\frac{2L_{wd}}{\pi}\frac{\partial p_d}{\partial y_d} = \begin{cases} -1 & \text{for } x_{wd}-L_{wh}\le x_d\le x_{wd}+L_{wh}. \\ 0 & \text{otherwise}, \end{cases} \tag{1.24}$$

This boundary condition is derived from (1.2) in the y direction

$$q_v = -\frac{kA}{\mu}\frac{\mathrm{d}p}{\mathrm{d}y}. \tag{1.25}$$

Taking a control volume infinitely close around the well 'strip' will give an area of

$$A = 2(2L_{wh}L_z). \tag{1.26}$$

Inserting (1.26) into (1.25) and non-dimensionalizing p and y gives

$$q_v = \left(-\frac{k_y 4L_{wh}L_z}{\mu}\right)\left(\frac{q_v\mu}{2\pi L_z\sqrt{k_x k_y}}\right)\left(\frac{\sqrt{\frac{k_x}{k_y}}}{Lx}\right)\frac{\partial p_{wd}}{\partial y_d}, \tag{1.27}$$

which can be rearranged to yield the desired boundary condition (1.24). A vertical skin S_{zd} is used as a proxy for the effect of flow in the z direction.

After derivation, the final analytical Kuchuk IPR solution for the above mentioned domain and boundary conditions is given by (1.28)

$$P_{wD} = \frac{2\pi L_y}{L_x}\sqrt{\frac{k_x}{k_y}}\left(\frac{1}{3} - \frac{y_w}{L_y} + \frac{y_w^2}{L_y^2}\right) + \frac{2L_x^2}{\pi^2 L_{wh}^2}\sum_{n=1}^{\infty}\frac{1}{n^3}\left(\sin\left(n\pi\frac{L_{wh}}{L_x}\right)\cos\left(n\pi\frac{x_w}{L_x}\right)\right)^2(1+\xi) + S_{zD}. \tag{1.28}$$

The parameters in (1.28) are found in (1.29) through (1.32):

$$S_{zD} = -\frac{L_z}{2L_{wh}}\sqrt{\frac{k_x}{k_z}}\left[\ln\left(\frac{2\pi r'_w}{L_z}\sin\left(\frac{\pi z_w}{L_z}\right)\right) + \sqrt{\frac{k_x}{k_z}}\frac{L_z}{L_{wh}}\left(\frac{1}{3} - \frac{z_w}{L_z} + \frac{z_w^2}{L_z^2}\right)\right], \tag{1.29}$$

$$r'_w := \frac{r_w}{2}\left(1 + \sqrt{\frac{k_w}{k_y}}\right), \tag{1.30}$$

$$\xi := \frac{2e^{\gamma L_y} + e^{\gamma(L_y - y_w)} + e^{\gamma y_w}}{1 - e^{\gamma L_y}}, \tag{1.31}$$

$$\gamma := -\frac{2n\pi}{L_x}\sqrt{\frac{k_x}{k_y}}. \tag{1.32}$$

The dimensionless pressure is then inserted into the equation for the productivity index

$$J = 2\pi \frac{\sqrt{k_x k_y} L_z}{\mu B_o (P_{wD} + S_m^*)}. \tag{1.33}$$

Here the skin has been scaled according to

$$S_m^* = \frac{h}{2L_h} \sqrt{\frac{k_x}{k_y}} S_m. \tag{1.34}$$

Summarizing, the assumptions made in the Kuchuk model are

- Steady state, single phase, isothermal and incompressible flow
- Homogeneous non-isentropic medium
- Horizontal box reservoir, no gravitational effects, principal flow directions parallel to axis
- Long perforation with respect to Lz (Goode & Kuchuk [1991])
- No wellbore pressure drop

In particular the assumptions of a homogeneous medium and zero wellbore pressure drop are constraining factors for production technologists Hill & Zhu [2006]. A discretized model can be used as alternative.

1.2.3 Discretized Model

The analytical solution derived by Kuchuk can also be tackled with a discretized model. The discretized model used in this thesis solves solves multiphase black oil equations. In Appendix A.1 it is shown that when these are solved for a single phase fluid, the equations reduce to the familiar form of (1.4) and (1.5), written again for convenience:

$$\mathbf{u} = \frac{-1}{\mu} \mathbf{k}(\nabla p), \tag{1.35}$$

$$\frac{\partial(\phi\rho)}{\partial t} = -\nabla \cdot (\rho\, \mathbf{u}) + q. \tag{1.36}$$

These equations are solved using a first order finite volume discretization. A Peaceman [1977] inflow model, described in Appedix A.2, is used to connect every perforated cell to the well network with Beggs and Brill pipe models. A detailed description of the wellbore network is given in Section 4.2. The entire well reservoir system is solved implicitly, using adaptive time stepping. After a time period of month, pseudo steady state flow is obtained and a comparison can be made with the Kuchuk IPR.

The assumptions of the usage of this specific discretized model are:

- Steady state, single phase, compressible isothermal flow
- Horizontal box reservoir
- Inclusion of gravitational force

Next to the Kuchuk and discretized model, there is a potential for intermediate fidelity IPR models.

1.2.4 Potential for an Intermediate Fidelity IPR

The Kuchuk model is limited because of its low fidelity wellbore treatment, and requirement on domain homogeneity. The discretized model has neither of these limitations, but in turn it is computationally expensive. An intermediate level of fidelity is envisioned, namely a Multi Point IPR (MIPR). This model is intended to have a more detailed wellbore inflow treatment, and can account for some reservoir heterogeneity, at a lower computational cost than the discretized model. The MIPR model is described in Chapter 4.

Chapter 2

Uncertainty Quantification

This chapter is an introduction to Uncertainty Quantification (UQ), in which the most important concepts are described that are necessary for solving the thesis research question. Section 2.1 addresses UQ terminology, Section 2.2 the concept of Bayesian inference, followed by Monte Carlo and Markov Chain Monte Carlo methods in Section 2.3 and 2.4. The specific implementation of these concepts can be found in Chapter 6. This chapter finishes with a section on examples of UQ in the domain of reservoir engineering and production technology.

2.1 UQ Concepts

Uncertainty Quantification "is the science of quantitative characterization and reduction of uncertainties in applications" Iaccanrino et al. [2009]. The definition of uncertainty itself requires elaboration. According to "AIAA guide for the verification and validation of computer fluid dynamics simulations" [1998], uncertainties are defined as "potential deficiency that is due to the lack of knowledge", as opposed to errors, which are "recognizable deficiencies of the models or the algorithms employed". Examples of model errors are those caused by truncation errors in series expansions, and physical effects that are not modeled.

There are two flavors of uncertainty, namely aleatory and epistemic uncertainty. The first type is irreducible physical variability in a system. An example in the context of reservoir simulation would be geometrical properties far from the wellbore that cannot be measured. On the other hand, epistemic uncertainty "is a potential deficiency that is solely due to a lack of knowledge" Iaccanrino et al. [2009]. This uncertainty is reducible.

Two steps can be made to reduce the uncertainties in applications. Model verification is the "substantiation that a computerized model represents a conceptual model within specified limits of accuracy." The second step, validation, is the "substantiation that a computerized model within its domain of applicability possesses a satisfactory range of accuracy consistent with the intended application of the model." Schlesinger [1979]. For this thesis, only model verification is within the scope of the project.

2.2 Bayesian Inference

Epistemic uncertainty can be reduced by means of Bayesian inference Kennedy & O'Hagan [2000]. This consists of updating a hypothesis based upon evidence acquired by data. It is based upon Bayes' law (2.1)

$$p_x(x|y) = \frac{p_y(y|x)\rho_x(x)}{p_y(y)}. \tag{2.1}$$

The aim here is to obtain the posterior of the hypothesis x given data y. This is equal to the likelihood of the data $p_y(y|x)$ multiplied by the prior distribution $\rho_x(x)$, divided by the probability $p_y(y)$. The latter is a shorthand notation for

$$p_y(y) \propto \int_x p_y(y|x)p_x(x)\,\mathrm{d}x. \tag{2.2}$$

The process of removing a random variable from a distribution is called marginalization. The denominator can be removed from (2.1), leaving the proportionality

$$p_x(x|y) \propto p_y(y|x)\rho_x(x). \tag{2.3}$$

Two types of methods used to evaluate (2.3) are intrusive methods and non-intrusive methods. Intrusive methods, like polynomial chaos, require changes to the model code, whereas non-intrusive methods use multiple deterministic evaluations of the model. The benefit of intrusive methods such as that of Loeven & Bijl [2008] is that the computational efficiency can exceed that of non-intrusive methods. However, the large number of parameters present in the MIPR model requires the usage of non-intrusive methods. Two of these methods are the Monte Carlo, and Markov Chain Monte Carlo methods.

2.3 Monte Carlo

Evaluating (2.3) requires numerical integration, commonly over a high dimensional space. Using sampling at regular intervals can become prohibitively expensive because of the curse of dimensionality. Monte Carlo techniques offer a way around this curse of dimensionality. The integral can be approximated as

$$\int f(x)p(x)\,\mathrm{d}x \approx E\left(\frac{1}{N}\sum_{i=1}^{N} f(X_i)\right). \tag{2.4}$$

Here X_i denotes the random samples obtained from the prior distribution $\rho(x)$. The convergence of (2.4) is proportional to $1/\sqrt{N}$ Weinzierl [2000]. This is significant, as this convergence behavior is independent from the number of dimensions of x. A more sophisticated method exists to further reduce the number of samples required, namely the Markov Chain Monte Carlo method.

2.4 Markov Chain Monte Carlo

The samples X_i in equation 2.4 do not necessarily have to be independent. Markov Chain Monte Carlo (MCMC) is an extension of Monte Carlo by Metropolis et al. [1953] that utilizes this property. Essentially, it consists of constructing a chain by accepting or rejecting random steps that will eventually attain the desired stationary posterior distribution.

A good introduction to MCMC is found in Diaconis [2009]. In this article, Markov chains have a stationary distribution π,

$$\sum_x \pi(x)K(x,y) = \pi(y). \tag{2.5}$$

Here $K(x,y)$ is the matrix that defines the Markov chain, which determines the probability of step y taken from position x. Then the first theorem of Markov chains states that

> Theorem 1: *Let X be a finite set and $K(x,y)$ a Markov chain indexed by X. If there is n_o so that $K^n(x,y) \geq 0$ for all $n > n_0$, then K has a unique stationary distribution π and, as $n \to \infty$, $K^n(x,y) \to \pi(y)$ for each $x, y \in X$,* Diaconis [2009].

Thus, for large n, the Markov chain will approximate the target distribution $\pi(y)$. The initial steps taken from n_0 typically display a non-stationary 'burn-in' phase, before converging on $\pi(y)$. This part of the chain must be discarded.

Necessary properties of Markov chains are that these must be irreducible and aperiodic; all states should be reachable by the chain and the chain should not enter an infinite loop over a subset of states. Andrieu et al. [2003] Markov chains also display reversibility, in that the chain can move from x to y and back again.

Whereas Monte Carlo has a straightforward convergence behavior, this is not the case for MCMC, which is still an area of ongoing research. The mixing behavior of the chain can provide an indication of the number of steps required, where it is observed how readily the chain can move over the target distribution.

2.5 Application of UQ in Petroleum Engineering

Uncertainty Quantification is playing an increasing role in the domain of reservoir simulation, but is largely unused in the domain of production technology. The most common usage of UQ in reservoir simulation is the process of history matching. In this ill-posed inverse problem, subsurface parameters are updated according to field production data. Examples of history matching using UQ can be found in Abdollahzadeh et al. [2011] and Maschio et al. [2009]. An MCMC method is investigated by Hong & Sen [2008] using 4D seismic data. Ma et al. [2008] use a multi-stage MCMCM method. The author has been unable to find papers where UQ is applied in the domain of production technology. Expert consultation confirmed that UQ is not frequently used for IPR methods. This implies that the thesis topic has the potential to make a difference in this field.

Chapter 3

Problem Definition and Approach

3.1 Thesis Question Relevance

In asking the question whether a MIPR incorporating UQ can lead to a step change in completion design, it is essential to first understand why completion design matters for Shell.

As there are increasingly fewer hydrocarbon discoveries, it is imperative to develop existing fields as effectively as possible. Typically, the amount of hydrocarbons that can be extracted from a reservoir using primary recovery is on the order of 25% of the total hydrocarbons present Satter et al. [2008]. Increasing this percentage therefore has a significant potential. A number of options exist to increase the flow in (1.8), rewritten here for convenience:

$$q_v = \frac{kh(p_r - p_{wf})}{\mu B \left[\ln\left(\frac{r_e}{r_w} - 0.75 + s\right)\right]}. \tag{3.1}$$

Techniques such as steam flooding and polymer injection can change the average reservoir pressure, viscosity and relative permeability. Artificial lift such as gas injection can reduce the bottom hole pressure. Production technologists focus on selecting the best possible skin, and it is here where this research aims to make a contribution.

Currently there is a trend for more complex completions, which can cost up to one million dollars S. D. Joshi [1991]. A poorly designed completion requires rework, or can even render a well useless. Considerable uncertainty exists in the data on which the decision is made for a certain completion design. In Section 2.5 it is found that although sophisticated UQ exists in the domain of reservoir engineering, this is not yet the case for the domain of production technology. Given the costs involved when mistakes are made, this is a potential area of improvement.

An uncertainty quantified MIPR model could bring about a step change in completion design, not because it designs completions, but because it efficiently provides information

used to design completions. As it is computationally efficient, it will provide production technologists with data earlier on in a project. For instance, provide a quick prediction before an expensive discretized model run is started. The latter is relevant, as Shell currently aims to integrate multi-fidelity reservoir and production technology tools into one single computational framework. Making use of this integrated approach, this thesis research aims to extend the UQ techniques of Chapter 2 into the production technology domain.

3.2 MIPR UQ Approach

For a MIPR incorporating UQ to provide a step change in completion design, three aspects have to be demonstrated. First of all, it must first be shown that MIPR and its Kuchuk zones are valid models and are candidate substitutes for a discretized model. This is accomplished in Chapter 4 and 5. Secondly, it must be demonstrated that UQ techniques can be used to calibrate a MIPR model.

As a MIPR model divides the perforation up into zones, the data should also be obtained at several measurement stations in the perforation. With the advent of fiber optic measurements as described in Section 1.1.2, this is now a possibility. Fiber optic measurements are an expensive state-of-the-art measurement technique, hence work in this area has been performed in research rather than field wide operations. As surrogate, a discretized 'truth model' will supply synthetic fiber optic measurements. The MIPR UQ based on this data will be performed in Chapter 6.

Lastly, it should be shown that the productivity index predictions of the UQ MIPR are sound. As a discretized 'truth model' is used for the creation of data, this same model can be used to provide 'truth predictions' to compare results with. This is accomplished in Chapter 7.

Part II

MIPR Uncertainty Quantification and Calibration

Chapter 4

MIPR Model

In this chapter a description of the MIPR model is given. After the introduction in Section 4.1, the mechanics of the model are described in Section 4.2. Section 4.3 compares the assumptions of the MIPR model with those of a single-zone Kuchuk IPR and a discretized model.

4.1 Introduction to MIPR

The assumptions of a Kuchuk IPR are limiting for production technologists. For long horizontal wells, the wellbore pressure drop cannot always be neglected Novy [1995]. Furthermore, the reservoir is often inhomogeneous in nature. This can require different completion designs per section of the perforation. A discretized model is an alternative, albeit at a larger computational cost and set-up time.

An intermediate level of fidelity, incorporating heterogeneity, is intended for production technologists who need an fast and flexible initial sizing tool. This proxy can then be used before detailed analysis is performed in a later stage of well development when discretized models are used. In literature, a variety of approaches can be found. Ryou et al. [1989] derived a multi-layered reservoir IPR for axial inflow into a vertical well. Lolon et al. [2008] derived a similar model for radial flow. Yudin & Lubnin [2011] investigated transient effects for a horizontal multi-layer well. An transient model used to infer skin distributions from a single gauge well test is made for a homogeneous reservoir by Al-Otaibi & Ozkan [2005].

4.2 MIPR Model Description

The Multi Point IPR model required by Shell for this thesis is intended to simulate horizontal wells in the pseudo steady flow regime, making use of Kuchuk IPR models. As pointed out in Section 1.2.1, the reason for the requirement of Kuchuk IPR models is

that these offer more degrees of freedom in the position of the completion with respect to the drainage area than that of older models. An illustration of a Multi Point IPR can be found in Figure 4.1.

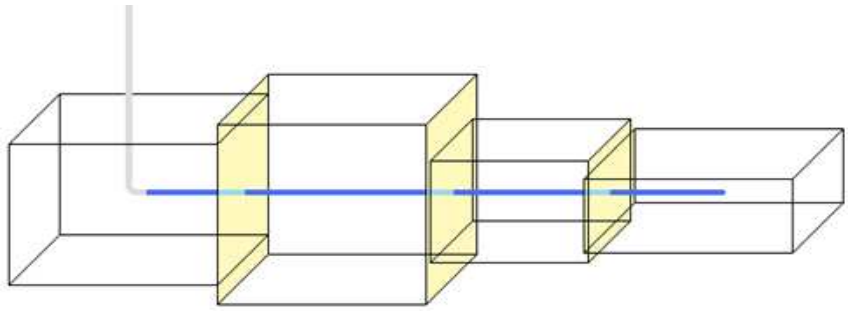

Figure 4.1: MIPR illustration

This model consists of several Kuchuk IPR models in series and can account for reservoir inhomogeneity and wellbore pressure drop, along with increased freedom in overall drainage area shape. Such a MIPR model can already be constructed from the tools available in the PROSPER production technology software, however, the author has not been able to find papers in which this particular model is verified.

An illustration of the wellbore network of an MIPR model with three zones is given in Figure 4.2.

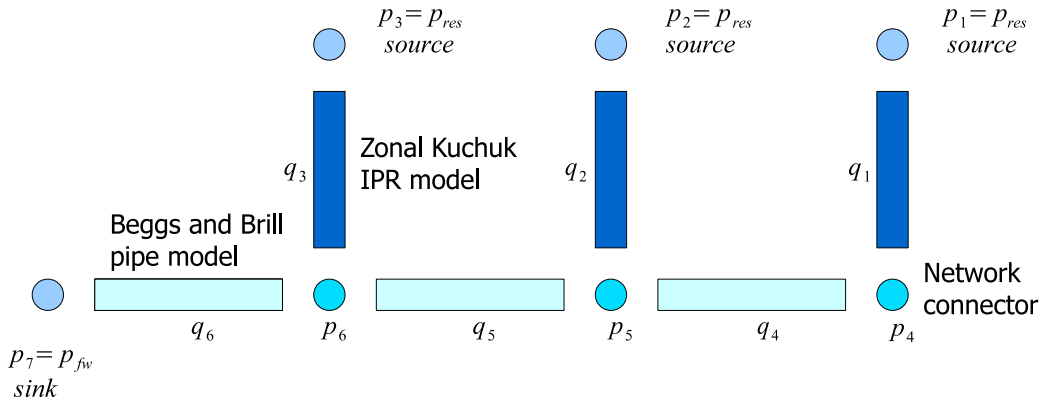

Figure 4.2: MIPR wellbore network topology with three zones

The circles at the top are sources in the reservoir, with fluids flowing through the network to the bottom hole, which acts as a sink. A network is represented by network connectors,

on which pressures live. The network connectors are linked by pipe segments, depicted as horizontal bars in Figure 4.2. Volumetric flow passing through a particular segment is represented as q_i. The vertical IPR segments lie in the reservoir and contain the Kuchuk IPR models, the equations of which have been described in Section 1.2.2.

4.2.1 Well Network Models

Pipe flow models are inserted into the pipe segments. Out of all pipe models described in Section 1.1.3, the empirical correlations found by Beggs & Brill [1973] are selected for this thesis. The reason for this is that these correlations are an industry standard, and because they differentiate themselves in that they can handle multiphase pipe flows at any pipe inclination. It is useful to give a brief description of the form of these correlations.

Beggs & Brill [1973] start their work with the energy equation

$$\frac{\mathrm{d}p}{\mathrm{d}Z} = -\left[\frac{g}{g_c}\rho_{tp}\sin\theta + \rho_{tp}\frac{\nu_m}{g_c}\frac{\mathrm{d}\nu_m}{\mathrm{d}Z} + \rho_{tp}\frac{\mathrm{d}w_f}{\mathrm{d}Z}\right], \tag{4.1}$$

which has the form of

$$-\frac{\mathrm{d}p}{\mathrm{d}Z} = \left(\frac{\partial p}{\partial Z}\right)_{el} + \left(\frac{\partial p}{\partial Z}\right)_{acc} + \left(\frac{\partial p}{\partial Z}\right)_{f}. \tag{4.2}$$

The respective terms on the right hand side of the equation are the potential energy gradient, kinetic energy gradient, and friction dissipation. After rewriting the terms in (4.1), the final energy equation is written as

$$-\frac{\partial p}{\partial Z} = \frac{\frac{g}{g_c}\sin(\alpha)[\rho_L H_L + \rho_g(1-H_L)] + \frac{f_{tp}G_m\nu_m}{2g_c d}}{1 - \frac{[\rho_L H_L + \rho_g(1-H_L)]\nu_m\nu_{sg}}{g_c p}}. \tag{4.3}$$

The parameters of (4.1) and (4.3) are given in Table 4.1. The two parameters in (4.3) that Beggs & Brill [1973] have found experimental correlations for are the liquid holdup H_L and the friction factor f_{tp}. The liquid holdup is defined as the cross sectional area of the pipe occupied by liquid flow. Extensive correlations have been found for H_L for all multiphase flow regimes, however, for the single phase flow of this thesis, H_L is simply equal to one.

Secondly, the friction factor is addressed. The correlation found for the no-slip friction factor is

$$f_{ns} = \left[2\log\left(\frac{N_{Rens}}{4.5223\log N_{Rens} - 3.8215}\right)\right]^{-2}, \tag{4.4}$$

where

$$N_{Rens} = \frac{[\rho_L\lambda + \rho_g(1-\lambda)]\nu_m d}{\mu_L\lambda + \mu_g(1-\lambda)}. \tag{4.5}$$

Parameter	Description
d	Pipe diameter
f_{tp}	Two phase friction factor
G_m	Mixture mass flux rate w/Ap
g	Acceleration due to gravity
g_c	Gravitational constant
H_L	Liquid holdup
w	Mass flow rate
w_f	Friction losses
Z	Coordinate along pipe
ρ_L	Density of the liquid phase
ρ_{tp}	Two phase mixture density $\rho_L H_L + \rho_g(1 - H_L)$
ν_{sl}	Superficial liquid velocity q_L/Ap
ν_m	Mixture velocity $(q_L + q_g)/Ap$
ν_{sg}	Superficial gas velocity q_g/Ap
θ	Pipe inclination angle from horizontal

Table 4.1: Parameters in pipe model

The no-slip friction factor is correlated with the two phase friction factor by parameter S:

$$\frac{f_{tp}}{f_{ns}} = e^S, \tag{4.6}$$

$$S = \ln(y^*)\left(-0.0523 + 3.182\ln(y^*) - 0.8725(\ln(y^*))^2 + 0.01853(\ln(y^*)^4)\right)^{-1}, \tag{4.7}$$

where y^* is defined by

$$y^* := \frac{\lambda}{(H_L(\theta)^2)}. \tag{4.8}$$

For a single phase fluid, $y^* = 1$, hence $S = 0$, from which it follows that $f_{tp} = f_{ns}$. With the description of the pipe models and that of the Kuchuk IPR model, the process of solving this network can be addressed.

4.2.2 Solution Process

The solution of the wellbore network in Figure 4.2 starts with imposing the boundary conditions. On each of the sources, the pressure and the type of fluid flowing into the network are specified. All pressures at the sources are set equal to the average reservoir pressure. The fluid is described using oil tables of the type found in Appendix B. It will be shown in Section 5.3 what repercussions this has. Finally, a bottom hole pressure is specified at the sink.

The entire network is solved implicitly, but it is useful to describe the solution process in an iterative manner. The first step is to assume a certain pressure in the wellbore. Each Kuchuk IPR model can then use the pressure difference to determine the volumetric flow q flowing through each Kuchuk IPR segment. Next, a control volume can be drawn around each network connector, in which conservation of mass holds. Consequently the flows through each of the pipe segments are known. These flows can then be inserted into the pipe model equation (4.3), which consequently calculates the pressure drop. Starting from the pressure at the bottom hole, each of the upstream network connectors can then have its pressure updated. From here the next iteration can start. One complication is that the fluid properties are pressure dependent, these are retrieved from tables for each individual pipe segment. This is also called a 'fluid flash' calculation. For the single phase fluid of this thesis, this nonlinearity is weak. Instead of the iterative description above, this thesis uses an implicit first order Newton-Rhapson solution method, which is detailed in Appendix A.3.

Significantly, when the MIPR model will be verified against discretized models, the same well network construction method is used. The number of network connectors and sources on the other hand will be larger. Instead of the Kuchuk zones, the wellbore network is attached to each perforated cell using a Peaceman inflow model described in Appendix A.2. Hence discrepancies between the two models can primarily be attributed to a different description of reservoir flow rather than wellbore flow, the former being the primary interest of this thesis.

4.3 MIPR Assumptions

Returning to Figure 4.2, each of the zones can accommodate its own permeability's and skins. At the expense of this increase of functionality, it requires the placement of no-flow boundaries between the different zones. Therefore, it assumes radial flow in all but the zones at either end.

The assumptions of the three models are compared in Table 4.2

Assumption	Kuchuk	MIPR	DM
Steady state	√	√	√
Single phase	√	√	√
Isothermal	√	√	√
Compressible	×	×	√
Gravitational force	×	×	√
Wellbore pressure drop	×	√	√
Principle flow directions on axis	√	√	√
Horizontal box domain	√	√	√
No homogeneous domain required	×	√	√
No long perforation required w.r.t. L_z	×	×	√
No artificial no-flow boundaries in domain	√	×	√

Table 4.2: Assumptions of the Kuchuk, MIPR and discretized model

Summarizing, the Kuchuk model does not incorporate a wellbore pressure drop or heterogeneity in the permeability. The MIPR model does not have these restrictions, however, this comes at the expense of artificial no-flow boundaries in the domain. A discretized model has neither of these two drawbacks. In Chapter 5, the effect of these different assumptions is investigated.

Chapter 5

MIPR Verification

Verification of the MIPR model can be achieved by several different means. The main challenge of verifying the MIPR model lies in the fact that it has a large number of parameters. The goal of the verification is to assess within which range the MIPR lies compared to a reference discretized model. For simple domains, a single zone Kuchuk model can be included as an extra model. Verifying the Kuchuk model itself is significant, as this model is used for each of the zones in the MIPR model.

The verification is performed in three steps. Firstly, the effect on the number of zones in a homogeneous permeability MIPR box domain is investigated with respect to a discretized model in Section 5.1. In this verification step, the gridding error of the discretized model will also be investigated. The second step in Section 5.2 will involve a similar homogeneous box verification between the three models, over the entire parameter space of the MIPR model. The last verification step in Section 5.3 will involve a more complex MIPR, with a different permeability in each zone, which is then verified against a discretized model with a similar domain.

5.1 Model Gridding Verification

In Section 5.1.1 the discretization error of the discretized model is analyzed. The effect of the number of zones of the MIPR model is investigated in Section 5.1.2. The quantity of interest is the productivity index. There are two kinds of productivity indexes; the overall PI, or the distributed PI, denoted as PI_L. The overall PI is the ratio of well flow and drawdown at the bottom hole location. The PI_L is a local PI per unit length of perforation.

5.1.1 Discertized Model Grid

A mesh convergence analysis is performed for a discretized model with parameters found in 5.1, which have been taken from the case studied by Goode & Kuchuk [1991].

Parameter	Value	Unit
k_x	4.93E-14	$[m^2]$
k_y	4.93E-14	$[m^2]$
k_z	4.93E-14	$[m^2]$
x_w	609.6	$[m]$
y_w	609.6	$[m]$
z_w	7.62	$[m]$
L_x	1219.2	$[m]$
L_y	1219.2	$[m]$
L_z	15.24	$[m]$
L_{wh}	457.2	$[m]$
s	0.0	$[-]$
r_w	0.0762	$[m]$
p_r	2.4821E7	$[Pa]$
p_{fw}	2.4132E7	$[Pa]$

Table 5.1: Verification domain of MIPR and discretized model gridding investigation

The black oil fluid used can be found in Appendix B. The effect on the number of cells on the PI is shown in Figure 5.1.

It is found that the PI error has converged to within 2.0E−11 % at 10,000 cells. For this study, an orthogonal grid of 14,415 cells is used: $[31, 31, 15]$. The slope of the line in Figure 5.1 is -0.9, confirming that a first order discretization is used. The outlier that is observed can be attributed to the effect when the ends of the perforation are only perforating a cell by a small length; for this point it was 9 meters as opposed to a cell length of 31 meters. Ultimately, this discretized model will not be convergent, as the Peaceman inflow model correlating the pressures in a perforated cell with the wellbore pressure will fail when cell length scales approach that of the wellbore radius.

The effect on the number of cells can also be observed on PI_L, as seen in Figure 5.2

It is observed that increasing the number of cells containing the perforation will cause the PI_L to converge to a U-shape profile. To either edge of the perforation, a hemispherical inflow is observed. Towards the center regions, radial inflow exists.

5.1.2 MIPR Zones

Increasing the number of MIPR zones has an entirely different response. Taking the same parameter set from Table 5.1, the overall PI zone convergence plot is displayed in Figure 5.3.

Unlike Figure 5.1, it does not converge when the number of zones are increased. It does, however, approximate the PI of $2.78\text{E} - 9$ calculated by the discretized model. An explanation for the curve in Figure 5.3 can be found when observing the effect on the distributed PI_L in Figure 5.4

It can be seen that the profile with only four zones mimics the discretized model better than that with 11 zones. This is because every zone introduces a new artificial no-flow

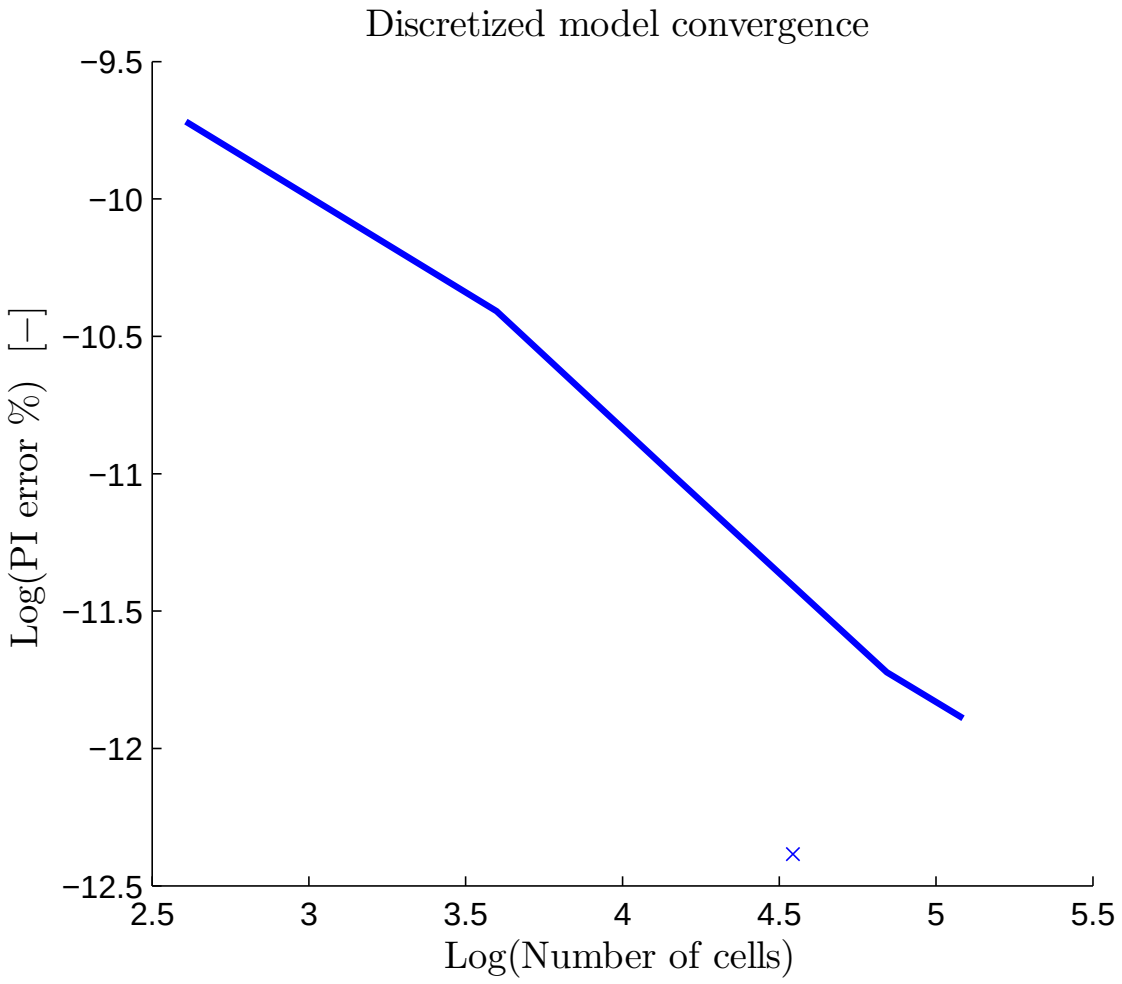

Figure 5.1: Discretized model grid convergence for PI

boundary in the domain. This causes the two end-zones to have hemispherical inflow, while the middle zones can only model radial inflow. Increasing the number of zones decreases the size of the zones at the end, meaning that the MIPR model assumes radial flow closer to the perforation edge than there is in reality.

After increasing the number of zones to 11, the PI begins to decrease again. What is being observed here is that the error in no-flow boundaries is being counteracted by the increased inflow resolution along the wellbore. In a Kuchuk model, the inflow occurs only at one point at the center of the perforation. In the MIPR model, increasing the zones will imply an increasingly more realistic inflow into the perforation. From the description of the wellbore network in Section 4.2, it is seen that there will be more pipe segments and more inflow points.

To conclude, it is found that the MIPR should be used with end-zones that contain a significant percentage of the perforation length. For this thesis, this is taken to be twenty percent.

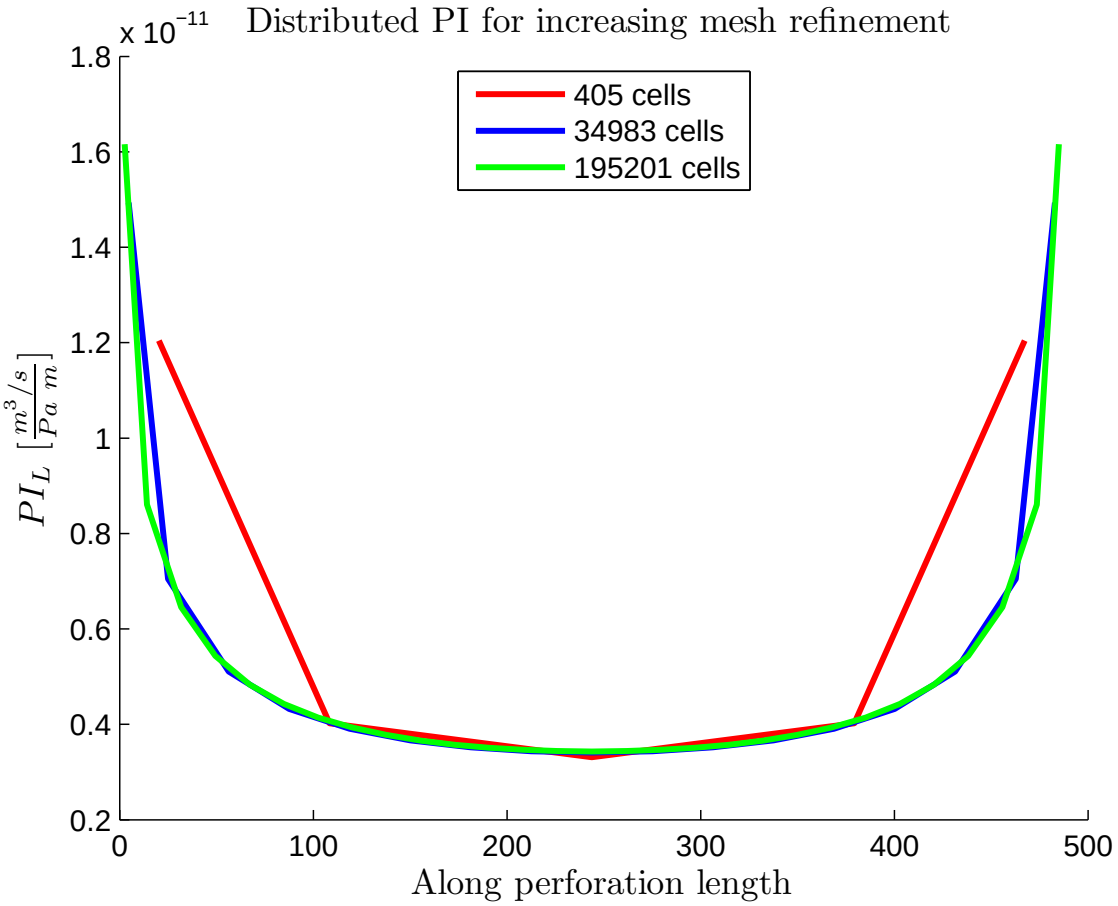

Figure 5.2: Discretized model grid convergence for PI_L

5.2 Homogeneous Drainage Area Verification

The verification of the MIPR model against the Kuchuk and discretized model is performed in two steps. Firstly, the effect of changes in individual parameters is studied. Later, a Latin hypercube sampling technique is applied to study the overall error for a certain parameter space.

5.2.1 Individual Parameter Verification

Four individual parameter variations are performed. The well position x_w, y_w and z_w are varied, and lastly the perforation length. The latter grows into the domain starting from one of the boundaries. A non-dimensional form will be used as in Table 5.2.

The results for changing these parameters are found in Figure 5.5. As expected, the Kuchuk model performs better than the MIPR model for this homogeneous case.

What can be seen in the figure in the top left hand corner, is that the MIPR performs best when the perforation is placed in the center. For the case of a perforation to the side of the drainage area, there is a large part of the end zone without a perforation. The

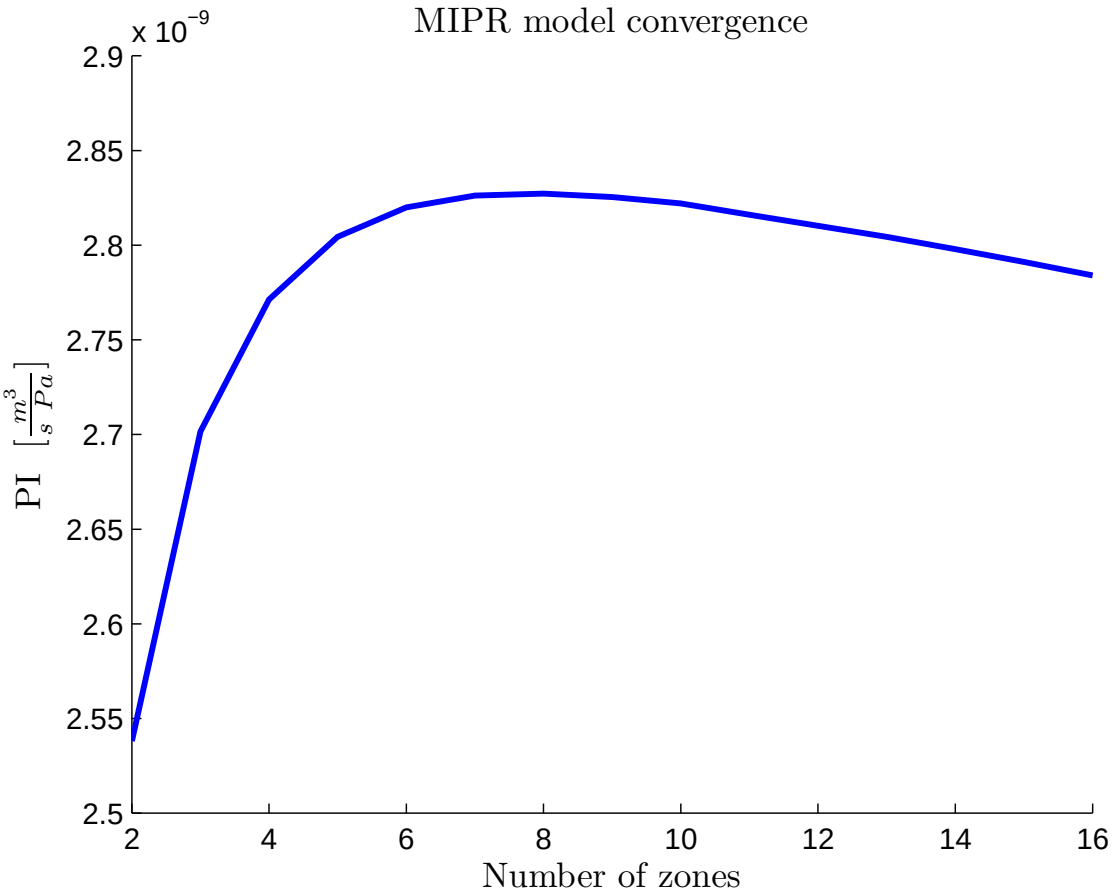

Figure 5.3: MIPR zone convergence for PI

Parameter	Definition	Value range
x_{wn}	$\frac{x_w - L_{wh}}{L_x - 2L_{wh}}$	0.05-0.95
y_{wn}	$\frac{x_y}{L_y}$	0.05-0.95
z_{wn}	$\frac{x_z}{L_z}$	0.05-0.95
$2L_{whn_s}$	$\frac{2L_{wh}}{L_x}$	0.05-0.95

Table 5.2: Non-dimensional parameter definition

zonal pressure used here is then too low, whereas the completely perforated zones have an average pressure that is too high.

When varying y_{wn}, the discretized model shows a reduction in PI as the perforation moves towards the top of the drainage box. The reason for this is the absence of a gravitational force in the Kuchuk and MIPR model.

The limitations of the MIPR model are best visible in the response to a change in the perforation length, as can be seen in the bottom right figure. When the perforation length is increased the PI increases linearly, as the average zone pressure is equal to the total average reservoir pressure. The Kuchuk and discretized model do not have this limitation,

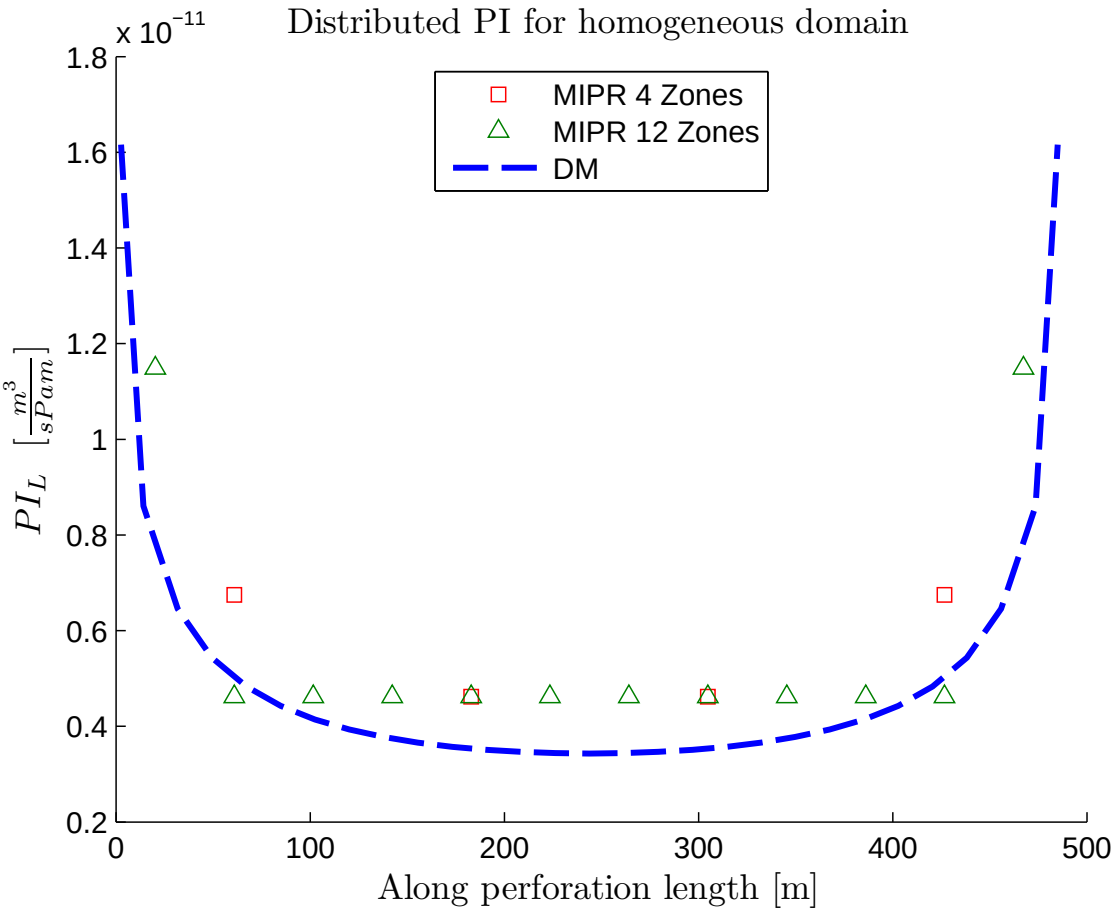

Figure 5.4: MIPR zone convergence for PI_L

and show a more curved response.

5.2.2 Latin Hypercube Sampling

In Section 5.2.1 it has been shown that the MIPR, Kuchuk and discretized models agree to within a certain PI range. To determine to which degree precisely, a Latin hypercube sampling method is utilized for the parameter space in Table 5.3, using a uniform distribution. A good description of Latin hypercube sampling can be found in Helton & Davis [2002].

Figure 5.6 shows the percentage offset in PI of Kuchuk and MIPR from the results of the discretized model. In this figure, the 10^{th}, 25^{th}, 75^{th} and 90^{th} percentiles are plotted, with the median represented by the horizontal bar in the center. It can be seen that the Kuchuk model systematically overpredicts the PI by about nine percent. From the model investigation in Chapter 4, this overprediction can be attributed to several effects, namely the assumption of incompressibility, gravity and wellbore dynamics in the Kuchuk model. The MIPR model performs worse; it overpredicts by around twenty percent, with a larger spread in results. This can be attributed to the incorrect assumption that the average

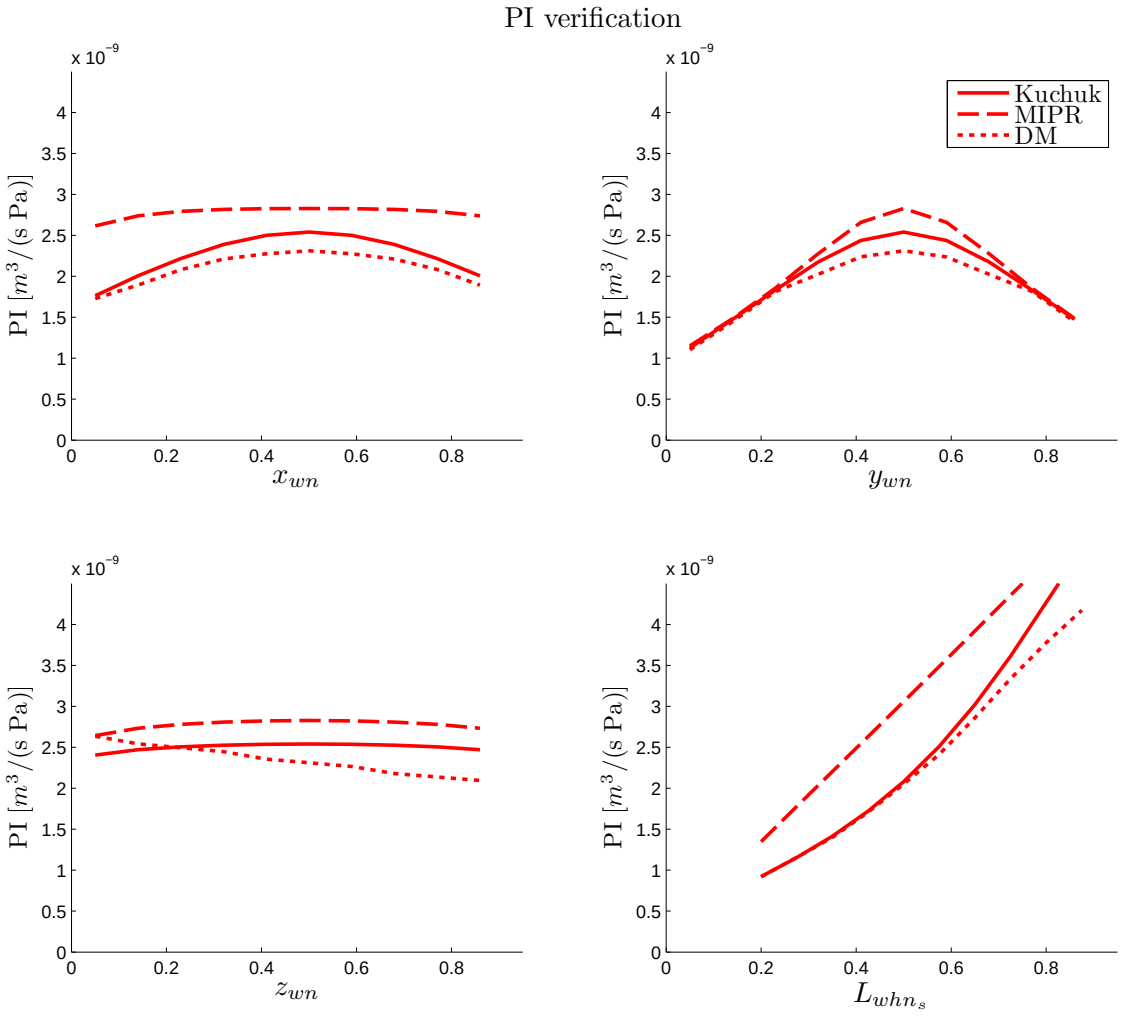

Figure 5.5: PI verification for individual parameters

Parameter	Min Value	Max Value	Unit
k_x	3.95E-14	5.92E-14	$[m^2]$
k_y	3.95E-14	5.92E-14	$[m^2]$
k_z	3.95E-14	5.92E-14	$[m^2]$
$x_{w_{nd}}$	0.4	0.6	$[-]$
$y_{w_{nd}}$	0.4	0.6	$[-]$
$z_{w_{nd}}$	0.4	0.6	$[-]$
L_x	1000	1400	$[m]$
L_y	1000	1400	$[m]$
L_z	14	16	$[m]$
$L_{wh_{nd}}$	0.3	0.5	$[-]$
s	0.0	2.0	$[-]$

Table 5.3: Verification sample space

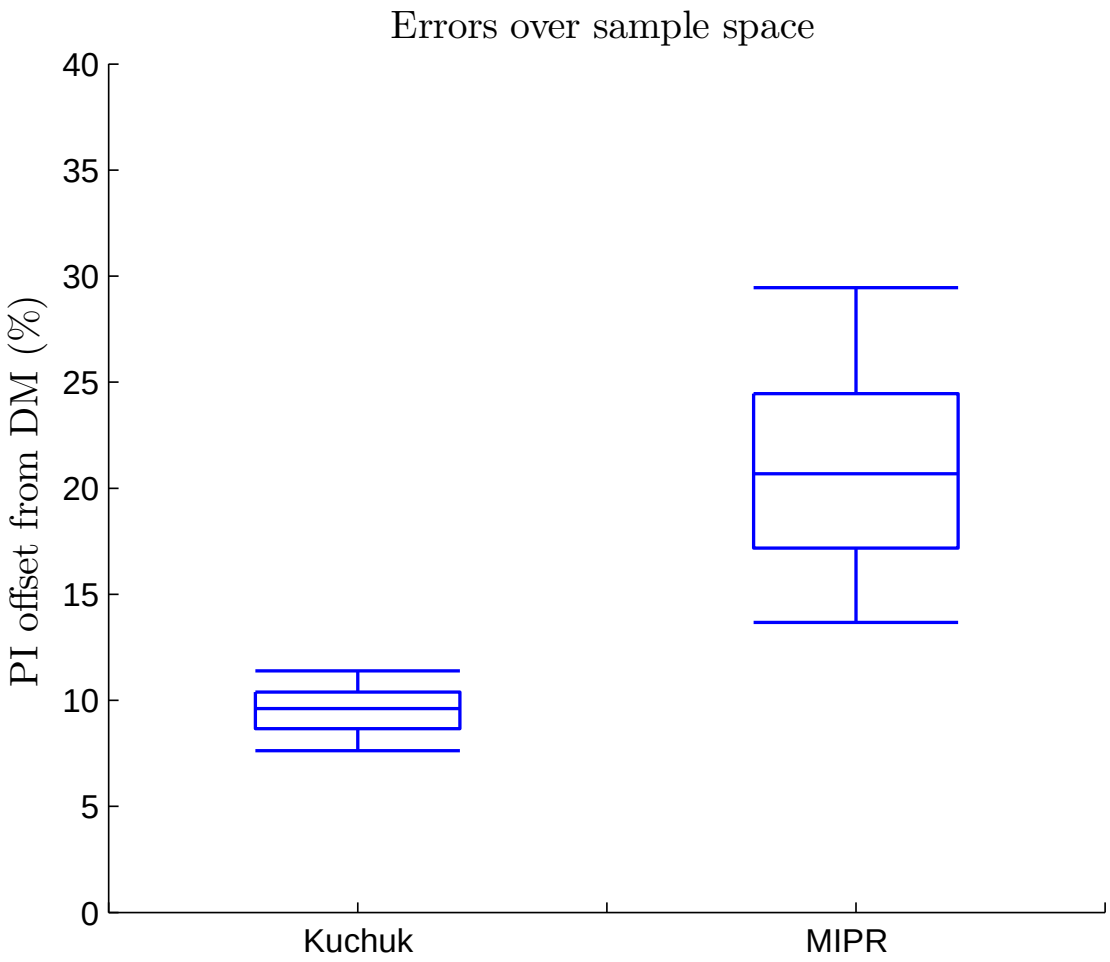

Figure 5.6: PI Kuchuk and MIRP percentage offset from a discretized model

zonal reservoir pressure is equal to the total average reservoir pressure, as will be shown in Section 5.3.

5.3 Heterogeneous Drainage Area Verification

In Section 5.2 a verification is performed for the homogeneous domain. However, MIPR is intended for use in cases where there are variations in zonal parameters. A verification over a domain with heterogeneity in the x direction is therefore required. The Kuchuk model can not be used in this case, thus a comparison is now only made between MIPR and the discretized model. These two models are constructed in such a way that the two domains are as similar as possible. The MIPR zone interfaces correspond with cell-to-cell interfaces in the discretized model. The range of cells corresponding to a MIPR zone have the same zonal permeability assigned. With this setup, the effect of zone-to-zone flow can be investigated. Tables 5.4 and 5.5 describe the parameter set over which the verification is performed.

Parameter	Unit	Value
L_x	$[m]$	2400.0
L_y	$[m]$	1600.0
L_z	$[m]$	22.0
x_w	$[m]$	1200.0
y_w	$[m]$	800.0
z_w	$[m]$	11.0
Ψ_h	$[-]$	1.0
Ψ_v	$[-]$	0.1

Table 5.4: Global heterogeneous verification domain of a MIPR and discretized model

Zone	L_{x_i} $[m]$	$2L_{x_i}$ $[m]$	k_{tot_i} $[Darcy]$
1	720	320	0.3
2	160	160	0.45
3	240	240	0.25
4	80	80	0.15
5	400	400	0.2
6	800	400	0.3

Table 5.5: Zonal heterogeneous verification domain of a MIPR and discretized model

In Table 5.4, Ψ denotes the permeability anisotropy. $\Psi_v = 0.1$ implies that the permeability in axial direction is ten times as large as permeability in horizontal direction.

The distributed PI_L plot can be seen in Figure 5.7. What can be observed for the MIPR model is that the PI_L profile shape shows a reasonable comparison with that of the discretized model, with the second end zone performing the worst. In this zone, which has the highest permeability, the MIPR model significantly overpredicts the PI_L. In Chapter 4, it is shown that the average zonal pressure equals the total average reservoir pressure. This assumption can be a source of error that can lead to this result. The average zonal pressures from the discretized model can be used to find the error in the MIPR drawdown, tabulated in Table 5.6.

Zone	1	2	3	4	5	6
MIPR drawdown error [%]	-6.55	14.76	13.88	10.76	6.19	-17.33

Table 5.6: Error in MIPR drawdown

A positive error means that the predicted drawdown is too large, and vice versa. Indeed, the assumption of a zonal average pressure equal to the total average pressure is large for the second zone. This makes sense, as a higher permeability would naturally cause the pressure to drop more than that of a low permeability region. For the last zone, the predicted drawdown is too small. With a correct MIPR drawdown, the MIPR prediction would actually be larger than it currently is.

These errors are in a sense unavoidable with the model in its current form. Corrections

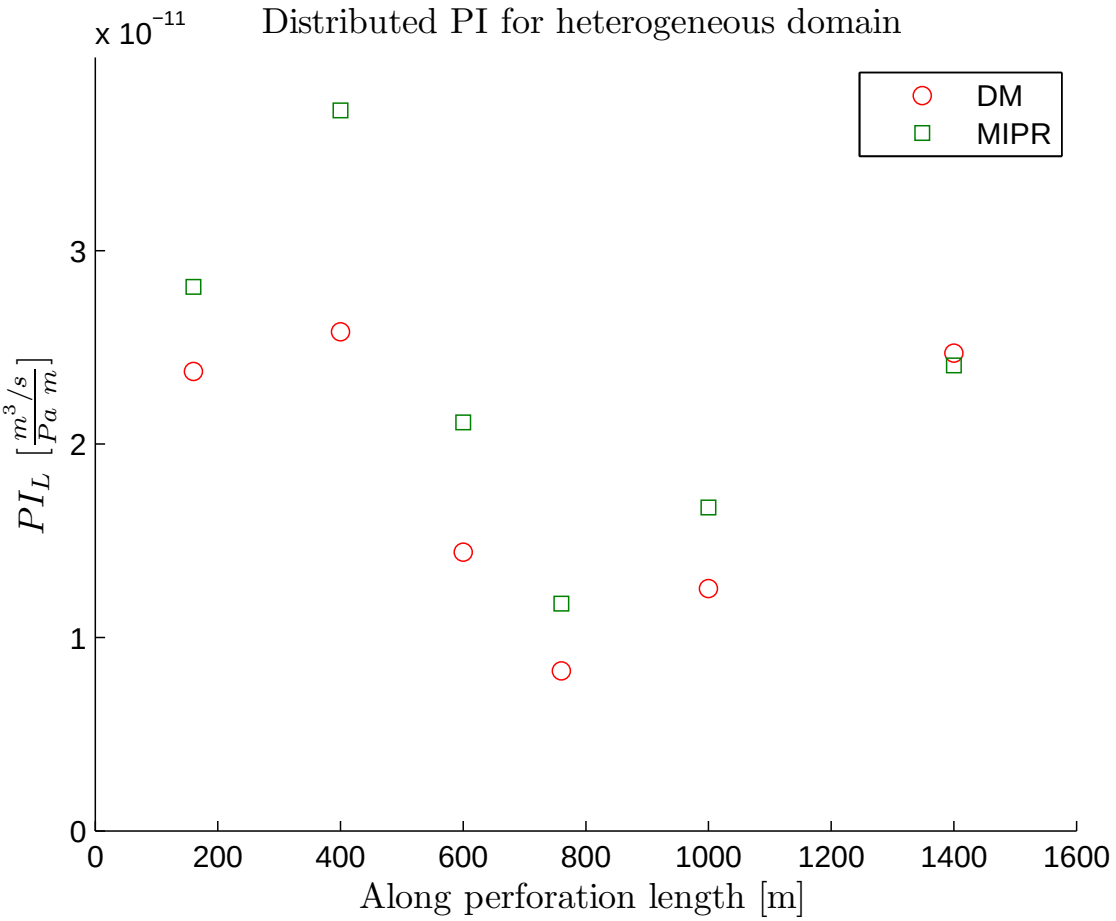

Figure 5.7: PI_L for MIPR and discretized model

can be made only when the solution is known, which would defeat the purpose of making these corrections. Model calibration is a solution to this problem, where artificial pressure drops in the form of skins can be inserted in to the Kuchuk model to correct for the errors in zonal drawdown.

5.4 Conclusion

It is found that for the homogeneous box domain of Table 5.3, the MIPR overpredicts the discretized model by around twenty percent when compared to a discretized model. A Kuchuk model has an overprediction of nine percent. Therefore, a MIPR model can used best only for those cases where reservoir heterogeneity along the x axis exists, and where an enhanced wellbore treatment is required. These results also imply that an MIPR model should ideally not be used as a completely stand-alone tool.

The MIPR model is not convergent, due to the placement of artificial no-flow boundaries in the domain. The length of end zones play a significant role in modeling the transition from hemispherical to radial inflow. For this thesis, the choice is made to let the length of the

perforation in the end zone be twenty percent of the total length of the perforation. This forms the main limitation on selecting the MIPR zones. The outcome of this verification is significant, as prior to this research, it was expected that zone-to-zone flow would be negligible. The verification work during this research will therefore have a large impact for customers of this model.

For a heterogeneous verification, MIPR shows a large overprediction with respect to the discretized model, which can primarily be attributed to the assumption that the average zonal pressure is assumed equal to the total average reservoir pressure. On the other hand, the actual shape of the PI_L distribution is similar.

It can be concluded that a uncalibrated MIPR by itself is useful, but not accurate enough to lead to a step change in completion design. In the next chapter, it is determined if this can be changed by introducing UQ.

Chapter 6

MIPR Calibration

In Chapter 5 it has been found that the MIPR model can be used as an intermediate fidelity model. The model has been shown to have a tendency to overpredict the PI on the order of twenty percent, for the particular experiment that has been performed. The model, if used as is, will therefore not facilitate a step change in completion design. It should then be determined if a MIPR model can be calibrated, and if this would then lead to a positive answer to the thesis research question.

In Section 6.1, the calibration approach is described. This is followed by a description of how UQ will be applied in Section 6.2. In Section 6.3, results of the calibration are presented. Lastly, in Section 6.4 an additional investigation into the MCMC method is made.

6.1 Calibration Approach

6.1.1 Model and Data

The heterogeneous model described in Section 5.3 is used for the calibration in this chapter. When performing a calibration, the data must have a form such that it can be predicted by the model to be calibrated for a chance of a unique solution. MIPR makes predictions of the PI_L at several points along the perforation. With the advent of fiber optic data, as described in Section 1.1.4, distributed productivity index measurements are becoming possible. As these techniques are still in an experimental phase, synthetic data will be used for thesis. For this, a discretized 'truth' model will be used. From the discretized model, PI_L distributions are obtained, to which measurement noise will be added.

6.1.2 Parameter Selection

The total list of model parameters in the MIPR model are $\{\mathbf{k_{x_i}}, \mathbf{x_w}, \mathbf{L_x}, L_x, \mu, B_o, \mathbf{s}\}$, whereas the primary variables are q_v and p. Here the subscript i denotes the zone in

question, while the remaining parameters concern the 'global' parameters. The MIPR parameters need to be placed into three sets; the epistemic parameters to be updated, the aleatory parameters, and parameters which are to be treated as deterministic.

As there is only one datum per zone, there should ideally be only one epistemic parameter to have a chance of a unique solution. The aim of the calibration is to reduce the model error. The parameters traditionally used to achieve this are calibration skins, denoted as s_β. These model the pressure drops caused by physics not resolved in the IPR model, such as non-radial flow. Alternative parameters, such as permeability, are not good candidates. Permeability's are already measured using well logs and other techniques mentioned in Section 1.1.4. Updating these parameters will not be very informative, as MIPR has a nontrivial model error that would need to be taken into account. It is best to update s_β, which represents the model error itself.

The remaining set of parameters is either aleatory or deterministic. The parameters μ and B_o are omitted from the set of aleatory parameters, as the black oil fluid used in DRMS does not lend itself for the parameterization within the constraints of the thesis project. Next, x_w and L_x are removed as well from the list, such that the grid and zones remain synchronized. Lastly, the three permeability's are reduced to one per zone to shorten the list and hence reduce the computational cost. This is accomplished by introducing an uncertain anisotropic permeability k that is multiplied with a fixed anisotropy. The uncertainties in the state parameters p_r, p_{wb_i} and q_i are represented as measurement uncertainty. Hence the aleatory parameter set α becomes

$$\alpha = \left\{ \begin{array}{c} k_i \\ L_y \\ L_z \\ y_w \\ z_w \end{array} \right\}. \tag{6.1}$$

These will then have the values in Table 6.1 and 6.2. According to the sources from Section 1.1.4, the length scales are proportional to the seismic data uncertainty. The permeability's have a distribution proportional to the measurement uncertainty of well logs.

Parameter	Unit	Value	σ
L_y	$[m]$	1600.0	80.0
L_z	$[m]$	22.0	0.1
y_w	$[m]$	800.0	5.0
z_w	$[m]$	11.0	0.05

Table 6.1: Prior distributions for the global domain

The prior of s_β is taken to have low informative value, as it has been found in Chapter 5 that there is a large spread in MIRP predictions:

$$s_\beta \sim N(0, 20)\ [-]. \tag{6.2}$$

Parameter	Unit	Value	σ
k_1	$[Darcy]$	0.3	0.01
k_2	$[Darcy]$	0.45	0.01
k_3	$[Darcy]$	0.25	0.01
k_4	$[Darcy]$	0.15	0.01
k_5	$[Darcy]$	0.2	0.01
k_6	$[Darcy]$	0.3	0.01

Table 6.2: Zonal prior permeability distributions

When inserted into the MIPR model, the prior contains the entire range of physically plausible PI_L predictions, as will be shown in Section 6.3.1. Finally, the measurement uncertainty is assumed to be that of (6.3)

$$\sigma_D = 1 \cdot 10^{-12} \ [PI/m]. \tag{6.3}$$

Fiber optic data is still in an experimental stage, and literature on measurement accuracy is scarce. After expert consultation, the author was advised to use the approximation in (6.3).

6.1.3 Sensitivity Study

A sensitivity study is performed to investigate the sensitivities of the epistemic and aleatory parameters. The effect on PI_L for the uncertainty distributions of Table 6.1 and 6.2 are investigated. In this sensitivity study, the skin is distributed as $s \sim N(0, 2)$. Only the results of the smallest and widest zone are plotted in Figure 6.1 and 6.2; that of zone four and six.

It is evident that PI_L is sensitive to s_β. The next most significant parameter is that of L_z, followed by k. The distribution in PI_L due to s_β is wider for the larger zone six. It is therefore expected that the calibrated skin distribution will be narrower for zone six than it will be for zone four.

6.1.4 Calibration Approach

The calibration is split up into two parts. The first part is a verification of the calibration method itself. For this, only measurement uncertainty is incorporated. The aleatory parameters identified in Section 6.1.1 are to be treated as deterministic. As the prior contains little information, it is expected that the predicted PI_L will have the means and standard deviations of the data.

The second calibration in Section 6.1.2 includes the full aleatory uncertainty. Here, it is expected that the predicted PI_L will have a larger spread than that of the data.

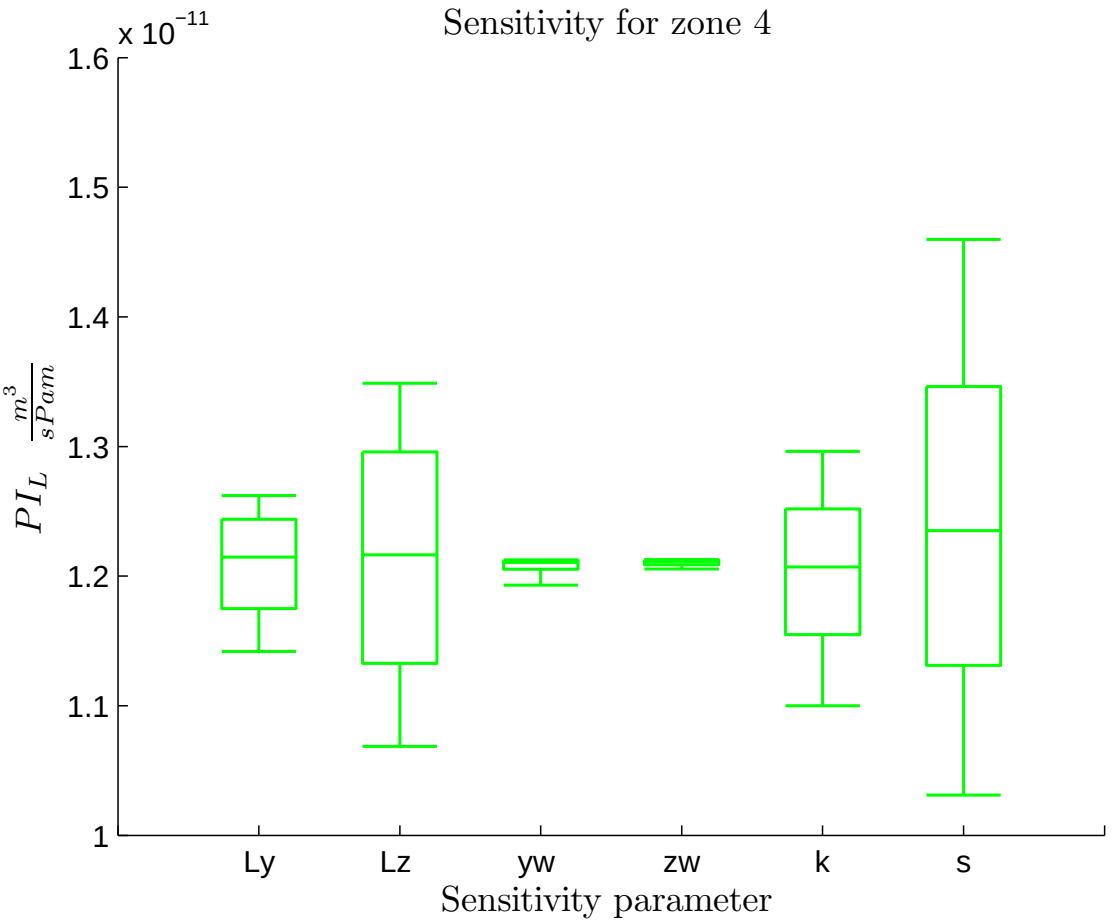

Figure 6.1: Sensitivity study for aleatory and epistemic parameters on PI_L for zone number four

6.2 Calibration Theory Application

In this section, the methodology for a deterministic calibration, and subsequently a stochastic calibration is outlined.

6.2.1 Deterministic Calibration

A deterministic calibration of a MIPR model using local fiber optic PI_L measurements can be accomplished analytically. The Kuchuk PI equation, (1.33) consists of two parts

$$J_M := \frac{c_1}{c_2}, \tag{6.4}$$

where

$$c_1 := \frac{2\pi\sqrt{k_x k_y}L_z}{B_o\mu}. \tag{6.5}$$

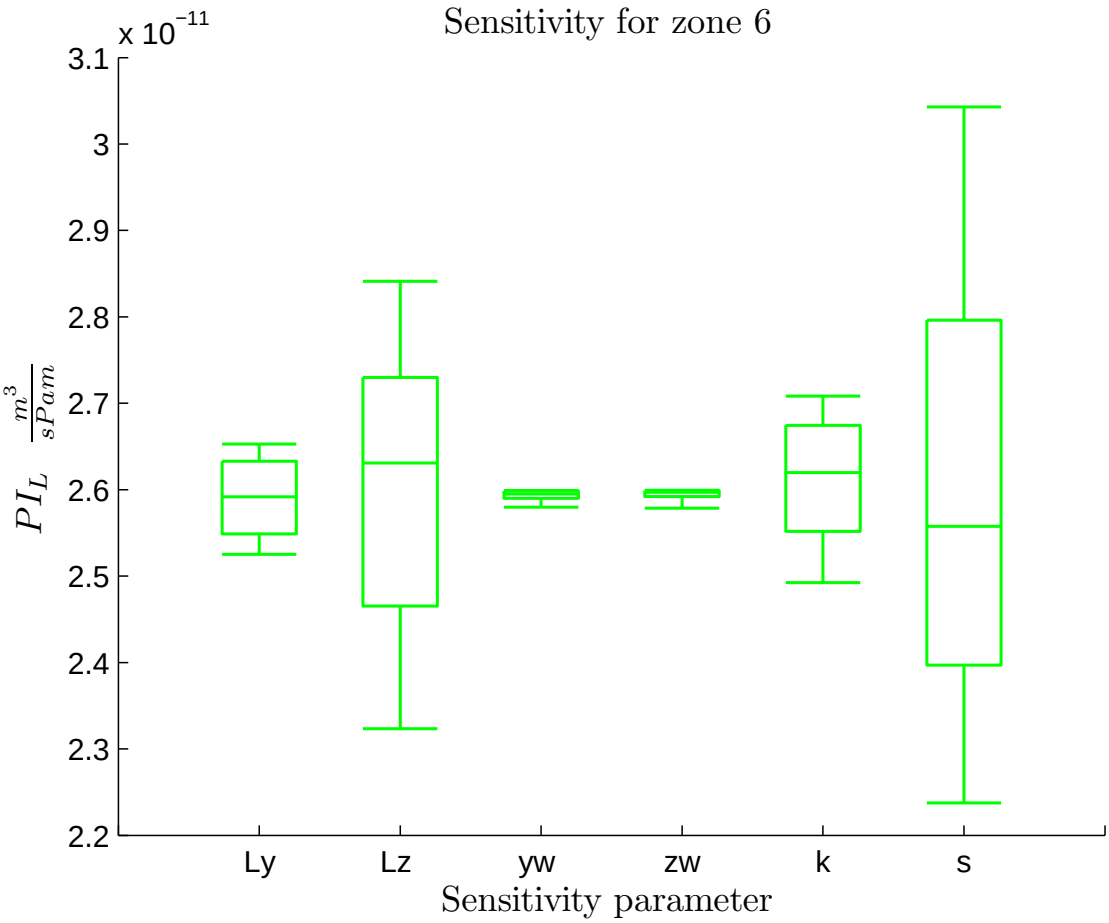

Figure 6.2: Sensitivity study for aleatory and epistemic parameters on PI_L for zone number six

This model should be calibrated with PI_L data obtained from measurements, J_D, by means of a calibration skin, s_{β_M}

$$J_D = \frac{c_1}{c_2 + s_{\beta_M}}. \tag{6.6}$$

Combining (6.4) and (6.6) and rewriting in terms of s_{β_M},

$$s_{\beta_M} = c_1 \left(\frac{1}{J_D} - \frac{1}{J_M} \right). \tag{6.7}$$

The subscript M stands for the MIPR model. Potentially, this method can also be used for the calibration of a discretized model in an iterative manner.

6.2.2 MIPR Bayesian Inference

The aim of the UQ MIPR is to use Bayesian inference to calibrate the model with data from fiber optic measurements. Bayes' rule found in (2.3) can be rewritten for the case

described in (6.7) as

$$p_{\beta_M}(\beta_M|J_D) \propto p_J(J_D|\beta_M)\rho_{\beta_M}(\beta_M). \tag{6.8}$$

Here β represents the set of epistemic calibration skins. The likelihood of $p_J(J_D|\beta_M)\rho_\beta(\beta_M)$ can be approximated by

$$J_D = J_M + \epsilon, \qquad \epsilon \sim N(0, \sigma_D^2), \tag{6.9}$$

where ϵ is the measurement error. Equation (6.8) can then be written as

$$p_J(J_D|\beta_M) \approx \exp\left(\frac{-(J_M(\beta_M) - J_D)^2}{2\sigma_D^2}\right). \tag{6.10}$$

In (6.10), σ_D is the standard deviation used to account for measurement uncertainty. The productivity index J_M is calculated for a set of deterministic domain and boundary parameters.

A more involved scenario is required to solve the thesis research question, as the aleatory parameter set α from Section 6.1.2 is included. Equation (6.8) is then written as

$$p_{\beta_M}(\beta_M|J_D \cap \alpha) \propto p_J(J_D|(\beta_M \cap \alpha))p_\alpha(\alpha|\beta_M)\rho_{\beta_M}(\beta_M). \tag{6.11}$$

Here the likelihood of $p_\alpha(\alpha|\beta_M)$ is equal to

$$p_\alpha(\alpha|\beta_M) = p_\alpha(\alpha). \tag{6.12}$$

This holds as $\alpha \perp \beta_M$; the prior belief is that the distributions of the calibration skins β are centered at zero no matter what the state of the aleatory parameters is.

In (6.11) the likelihood of $p_J(J_D|(\beta_M \cap \alpha))$ is written as

$$p_J(J_D|\beta_M \cap \alpha) \approx \exp\left(\frac{-(J_M(\alpha, \beta_M) - J_D)^2}{2\sigma_D^2}\right). \tag{6.13}$$

The marginalization of $p_J(J_D|\beta_M \cap \alpha)p_\alpha(\alpha)$ is addressed in Section 6.2.2.

MCMC With Aleatory Marginalization

The procedure for a MCMC approach to solve (6.11) using a Hastings [1970] transition kernel is written as follows

1. Set β_{M_i} to β_{M_0} at iteration $i = 0$
2. Generate candidate step β'_M from β_{M_i}, according to a normal distribution with a mean β_{M_i} and a variance tuned to generate the right acceptance ratio (20% to 50%).

3. Generate a random sample U from the uniform unit distribution $[0, 1]$

4. Evaluate

$$U \leq \min\left\{1, \frac{p_\beta(\beta'_M|(J_D \cap \alpha))p_\alpha(\alpha)p_\beta(\beta_{M_i}|\beta'_M)}{p_\beta(\beta_{M_i}|(J_D \cap \alpha))p_\alpha(\alpha)p_\beta(\beta'_M|\beta_{M_i})}\right\}, \tag{6.14}$$

   if this is true, accept the candidate step such that $\beta_{M_{i+1}} = \beta'_M$, set $\beta_{M_{i+1}} = \beta'_M$. Otherwise, $\beta_{M_{i+1}} = \beta_{M_i}$.

5. Continue previous three steps until a steady state solution is obtained. Discard the initial 'burn-in' part of the chain.

For the fourth step, an MC marginalization is performed over the space of α, for every β_M evaluation.

Partitioned Aleatory/Epistemic MCMC Marginalization

The evaluation procedure in 6.11 is computationally expensive. If the number of β iterations is N_β and for the MC marginalization N_α, then the total number of solves required is

$$N_{tot} = N_\beta N_\alpha. \tag{6.15}$$

For the MIPR model, one iteration takes 0.3 seconds, and for the discretized model this is up to ten seconds. An approach to reduce the number of iterations has been investigated, with mixed results, as will be revealed in Section 6.3.1.

Instead of the sequential approach with acquiring a new β and performing the marginalization, an integrated approach is desired with a single MCMC method with the state Φ:

$$\Phi = \left\{ \begin{array}{c} \alpha \\ \beta_M \end{array} \right\}. \tag{6.16}$$

Notice that state 6.16 includes both the aleatory and epistemic parameters. A traditional solution such an MCMC problem, where Φ' is obtained from Φ_i, would cause the aleatory parameters α to be updated as well, which is not desired. A solution to this problem is to treat α and β separately in a 'partitioned MCMC'.

1. Set Φ_i to Φ_0 at iteration $i = 0$

2. Generate candidate step β'_M from β_{M_i}, according to a normal distribution with a mean β_{M_i} and a variance tuned to generate the right acceptance ratio (20% to 50%) for a new chain step candidate.

3. Generate random sample α' directly from the distribution of α

4. Generate a random sample U from the uniform unit distribution $[0, 1]$
5. Evaluate

$$U \leq \min\left\{1, \frac{p_\beta(\beta'_M|(J_D \cap \alpha'))p_\alpha(\alpha')p_\beta(\beta_{M_i}|\beta'_M)}{p_\beta(\beta_{M_i}|(J_D \cap \alpha'))p_\alpha(\alpha')p_\beta(\beta'_M|\beta_{M_i})}\right\}, \tag{6.17}$$

   if this is true, accept the candidate step such that $\beta_{M_{i+1}} = \beta'_M$, set $\beta_{M_{i+1}} = \beta'_M$. Otherwise, $\beta_{M_{i+1}} = \beta_{M_i}$. Then $\Phi_{i+1} = \{\beta_{M_{i+1}}, \alpha'\}$. The α component of Φ does not need to be stored, as the stationary distribution of this is already known.
6. Continue previous three steps until a steady state solution is obtained. Discard the initial 'burn-in' part of the chain.

If the α component is drawn not from the previous step, but directly from its random distribution, it will have a stationary distribution as well, albeit uninfluenced by the data. The inclusion of α in Φ does increase the uncertainty in the posterior of β, as would be expected. If the number of samples N_Φ has the property that

$$N_\Phi \propto N_\beta, \tag{6.18}$$

then the performance increase has the proportionality of

$$\frac{N_{tot}}{N_\Phi} \propto \frac{N_\beta N_\alpha}{N_\beta} = N_\alpha. \tag{6.19}$$

The results of both MCMC approaches with aleatory marginalization are compared in Section 6.3.2.

6.3 Results Bayesian Inference

Before the results of the case with full aleatory uncertainty are presented, the case with only measurement uncertainty is addressed. This is a means to verify the calibration procedure.

6.3.1 Calibration Method Verification

The calibration that incorporates only measurement uncertainty is performed on the MIPR model. This provides a check to see if this model can indeed be calibrated with s_β. It is expected that the posterior distribution will correspond with that of the data.

The posterior and calibrated skins for the case where there is only measurement uncertainty are found in Figure 6.3.

It can be observed in Figure 6.3 that the posterior distributions of some calibration skins are larger than others, especially that of the fourth zone. This is because L_{x_4} is shorter than that of other zones, causing the PI_L to be less sensitive to a change in skin.

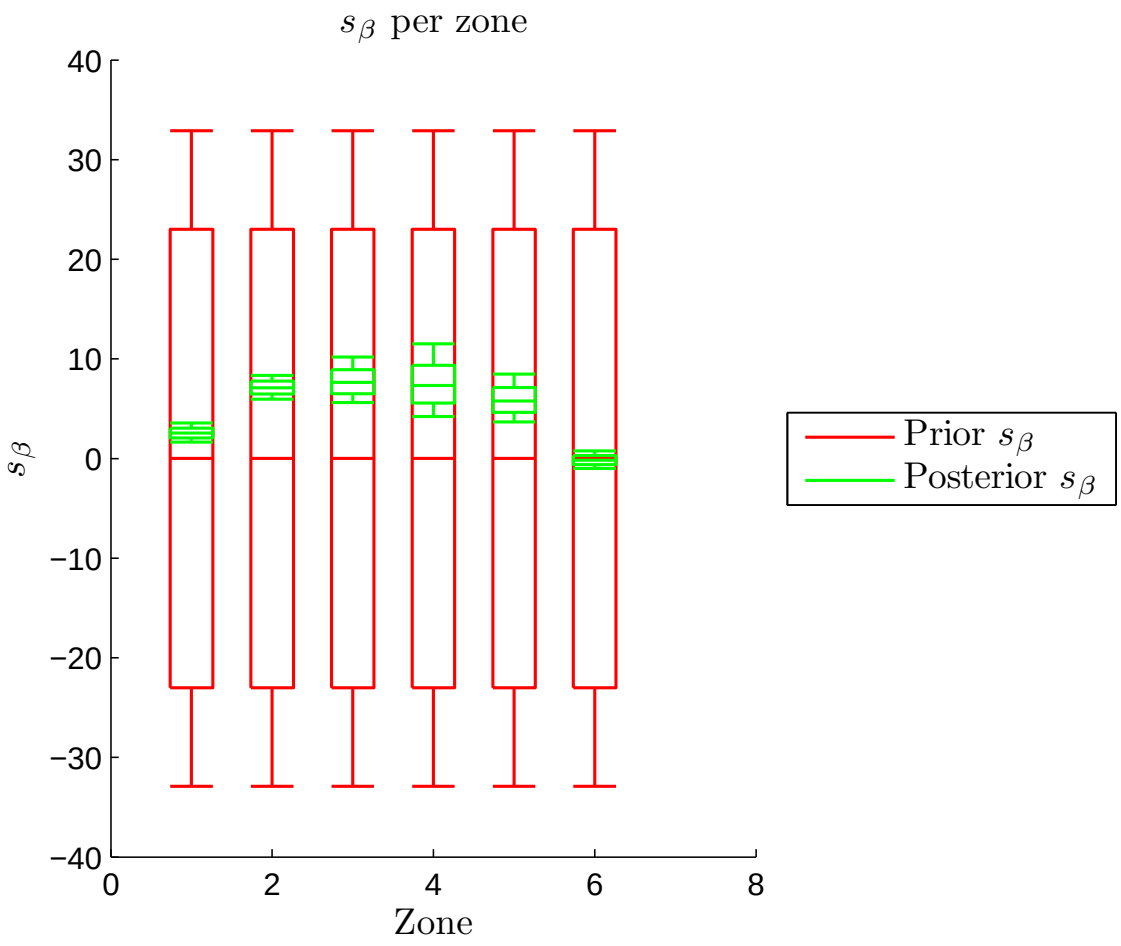

Figure 6.3: s_β with measurement uncertainty only, 19487 samples

In Figure 6.4, the predicted PI_L is shown. The range above the prior median has not been plotted. It is seen that the mean of the posterior coincides with that of the data, as the influence of the prior is small. As expected, the spread of the posterior approximates that of the data; it has a standard deviation of $1.0\text{E}-12$.

6.3.2 Calibration Results with Aleatory Uncertainty

Two approaches for determining the calibration posterior are investigated. The first is the conventional MCMC, where alpha is marginalized using MC for every MCMC step. The second is the 'pMCMC' method, as described in Section 6.2.2.

MIPR with Full Uncertainty

The calibration skins for a MIRP calibration with both epistemic and aleatory uncertainty are found in Figure 6.5.

The number of MCMC steps is 2984, each with an MC integral of 25 samples. The latter

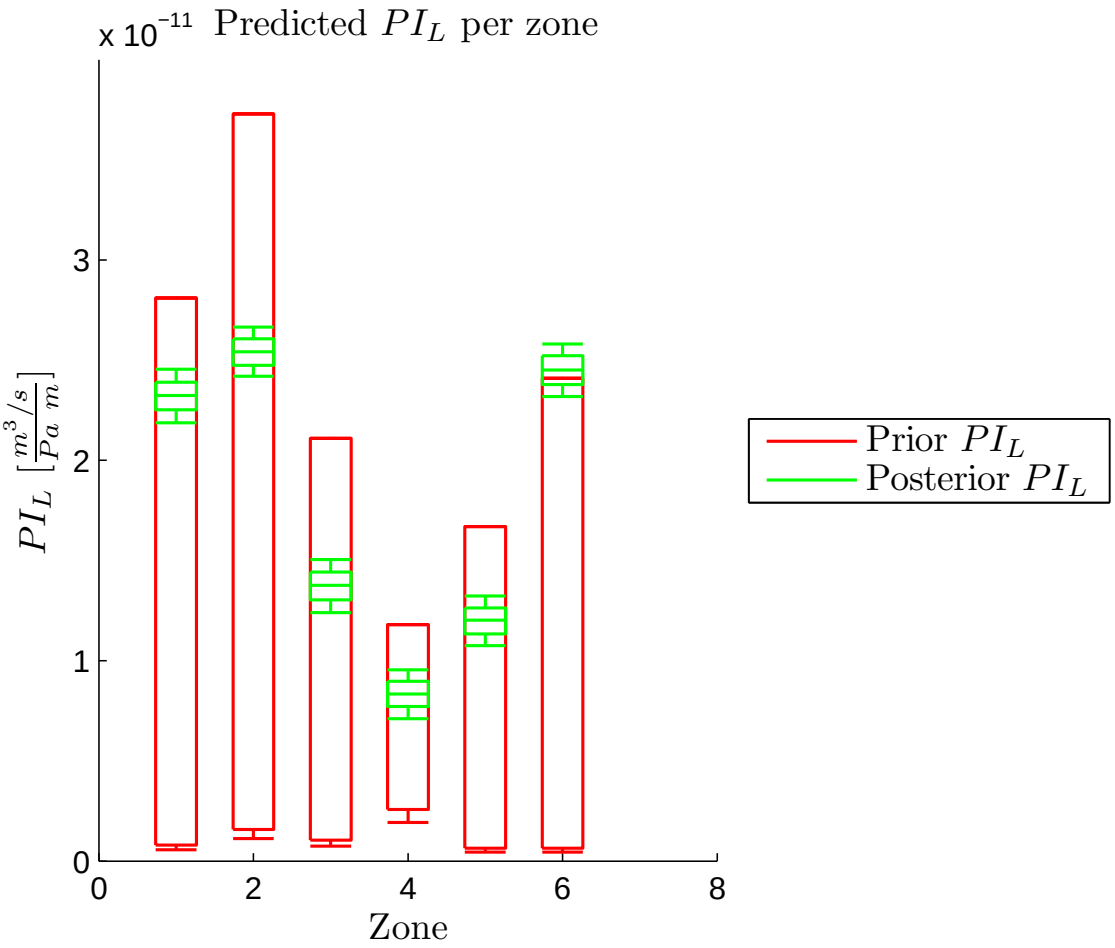

Figure 6.4: Predicted PI_L with measurement uncertainty only, 19487 samples. The uppermost line of prior represents the median, the region above has not been plotted

is taken to be small to limit the computational cost. The subsequent PI_L prediction is depicted in Figure 6.6.

It can be seen that the predicted PI_L posterior has a larger spread than that of the data, as the combined aleatory and measurement uncertainty is larger than just that of the measurement uncertainty. For some zones, the median of the data is slightly lower than the median of the prediction. This can be attributed to the slight effect of the prior distribution.

pMCMC Evaluation

The calibration skins using the pMCMC method are found in Figure 6.7.

The posterior distribution is close to that of the MCMC approach, but shows slight differences in distributions and median values. This does not necessarily mean that the results of pMCMC are incorrect. These slight differences could potentially be attributed to residual errors that could be reduced if more computational power is available and the

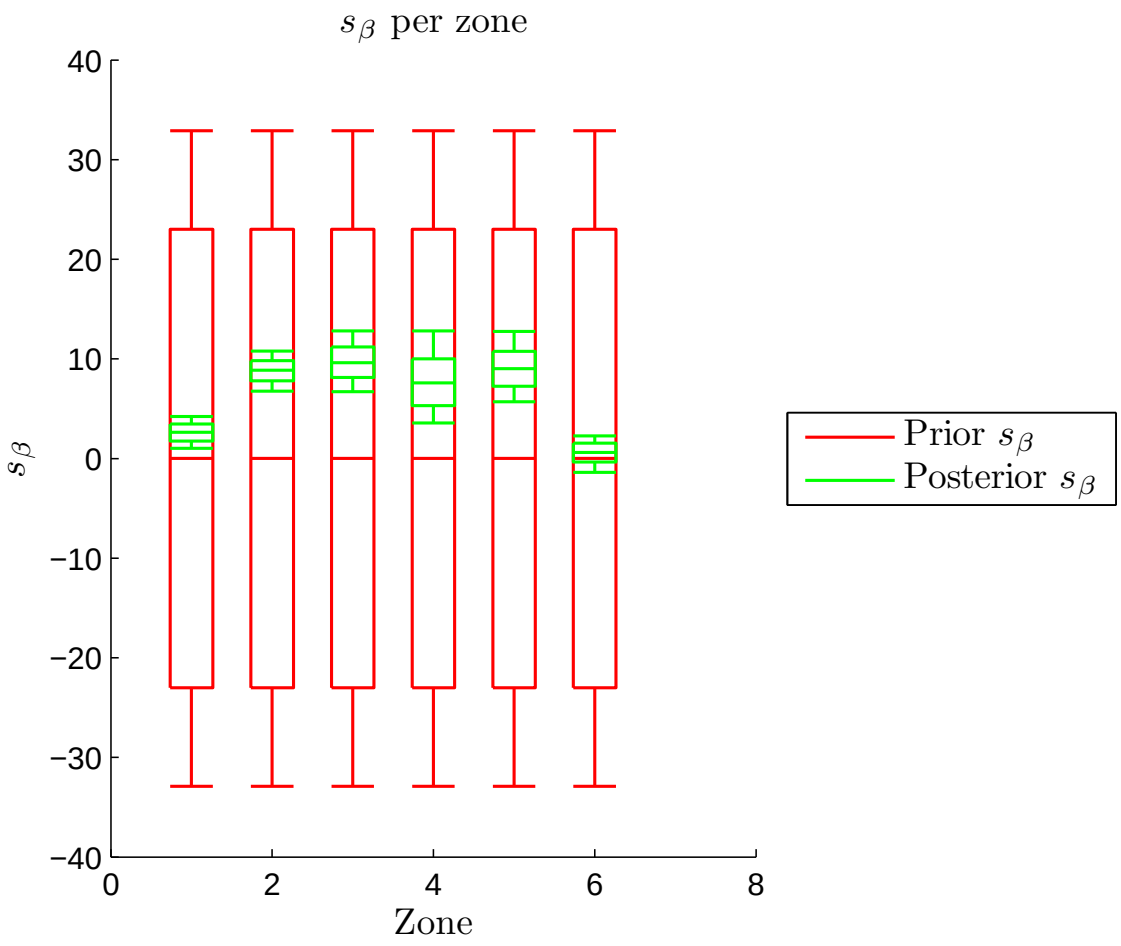

Figure 6.5: s_β with full uncertainty, 2984 MCMC samples

number of MCMC steps is increased. A further investigation into pMCMC is required to reach a conclusion, which is performed in Section 6.4.

6.4 Analysis of pMCMC

The pMCMC and MCMC method have both been used to calibrate the MIPR model, with only slight differences observed between these two methods. In this section, an additional investigation into pMCMC is performed to conclude whether this method can be used or not. First of all, the effect on the acceptance of a step is investigated in Section 6.4.1. Secondly, a simple problem is used to observe the difference between MCMC and pMCMC in Section 6.4.2.

6.4.1 Step Acceptance Comparison Between MCMC and pMCMC

In this section it is shown that that there is indeed a difference in the acceptance criterion between the MCMC and pMCMC model.

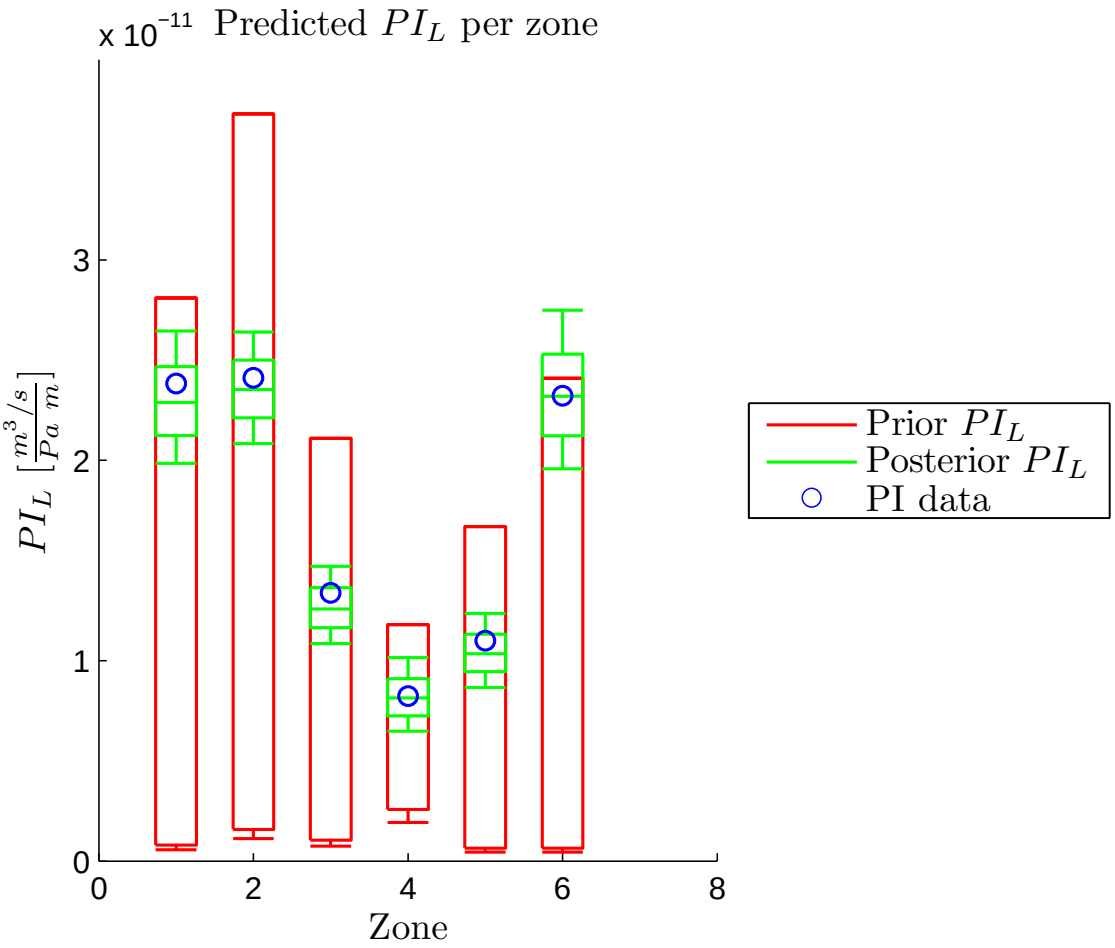

Figure 6.6: Predicted PI_L for full uncertainty, 2984 samples. The uppermost line of prior represents the median, the region above has not been plotted

Say the state X_i is the same for both MCMC and pMCMC. A candidate step Y as in Figure 6.8 is evaluated using the two methods. A sample U_0 is drawn from the uniform unit distribution [0,1]. For MCMC, the acceptance Boolean ξ will be

$$\xi_{MCMC}(X_i, Y, \alpha, (U_0 < U_{acc})) = \text{false}, \tag{6.20}$$

$$\xi_{MCMC}(X_i, Y, \alpha, (U_0 > U_{acc})) = \text{true}. \tag{6.21}$$

Here U_{acc} is the smallest value of U_0 to lead to the acceptance of the new step for the MCMC method.

In the case of pMCMC, there is a subtle difference. The acceptance criterion is now a function not of the distribution α, but a particular sample drawn from this distribution, α_N:

$$\xi_{pMCMC}(X_i, Y, \alpha_N, U_0). \tag{6.22}$$

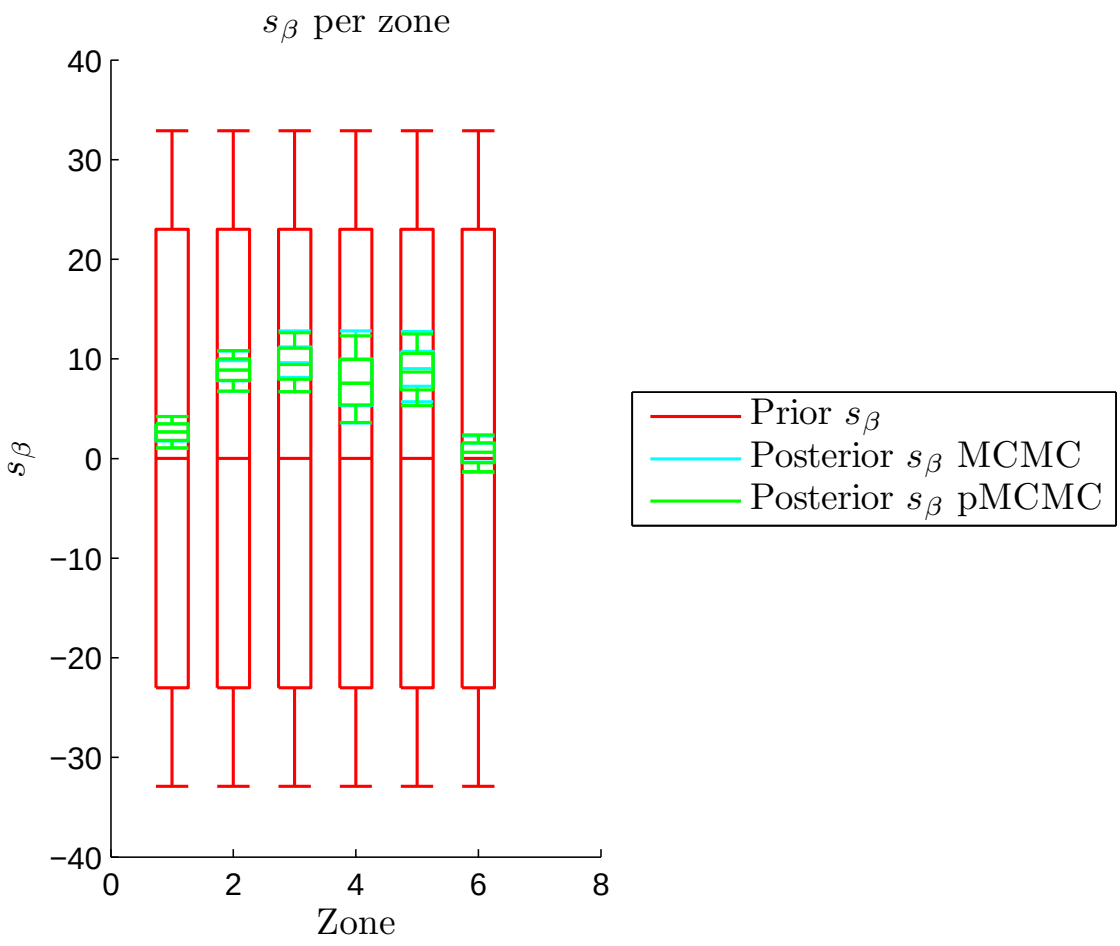

Figure 6.7: s_β with full uncertainty calculated with pMCMC, 16489 samples

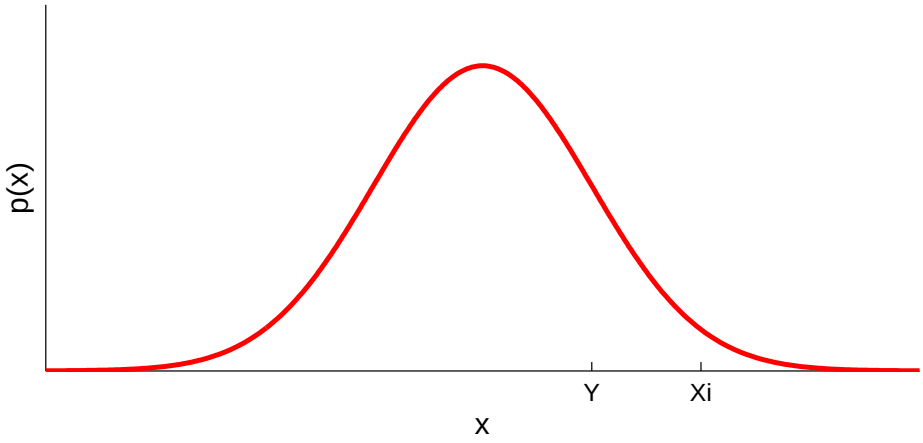

Figure 6.8: Candidate steps

Now as α is Gaussian, there is a subset $\widehat{\alpha_1} \subseteq \alpha$, from which an $\alpha_N \in \widehat{\alpha}$ is drawn, such

that

$$\xi_{pMCMC}(X_i, Y, \alpha_N, U_0) = \text{true} \qquad \text{for } \alpha_N \in \widehat{\alpha_1} \text{ and } (U_0 < U_{acc}), \tag{6.23}$$

$$\xi_{pMCMC}(X_i, Y, \alpha_N, U_0) = \text{false} \qquad \text{for } \alpha_N \notin \widehat{\alpha_1} \text{ and } (U_0 < U_{acc}). \tag{6.24}$$

Where U_{acc} is retained from the previous MCMC example.

Casually speaking, the set of $\widehat{\alpha}$ is a region with low likelihood that dominates over the fact that the candidate epistemic state increases the likelihood. What this demonstrates is that there is a chance that the pMCMC can take steps which would not have been taken with the MCMC method. Significantly, while the acceptance criterion is different, it does not necessarily imply that the posterior distributions are different as well for both methods. Possibly, these different steps can cancel in such a way that the same distribution is attained. From here there are two ways to verify the pMCMC method, one using more experiments, and secondly, a mathematical proof. The author has continued with experimentation, and recommends the proof for follow-up research.

6.4.2 Simple pMCMC Experiment

The outcomes of MCMC and pMCMC in Section 6.3.2 show a small difference that can be explained either by an error in the methods, or a residual effect due to limited samples having been taken. In this section, a computationally inexpensive problem is used to compare the two methods.

Let f be a model composed of two random variables a and b:

$$f = a + b \tag{6.25}$$

Where the prior distributions of a and b are both unit normal distributions

$$\rho(a) \sim N(0, 1), \tag{6.26}$$
$$\rho(b) \sim N(0, 1). \tag{6.27}$$

Say that an observation f_d is made on f, where

$$f_d \sim N(0.5, 1.5) \tag{6.28}$$

If a and b are both treated as epistemic, these can be updated to find the posterior distributions

$$p(a|f_d) \sim N(0.1169, 0.8745), \tag{6.29}$$
$$p(b|f_d) \sim N(0.1177, 0.8740). \tag{6.30}$$

Note that because of the symmetry in (6.25), both posterior distributions are equal, save for a small residual.

Now let a be aleatory, and only b epistemic. Several experiments are done, each with 1E7 samples, but some with a larger number of samples in the a plane. The results for the posterior b distribution are found in Table 6.3.

# MC samples # MCMC samples	1 (pMCMC) 1E7	10 1E6	100 1E5	1000 1E4
mean experiment set 1	0.1334	0.1327	0.1250	0.1590
mean experiment set 2	0.1335	0.1330	0.1346	0.1362
mean experiment set 3	0.1341	0.1323	0.1380	0.1286
mean experiment set 4	0.1329	0.1331	0.1337	0.1102
σ experiment set 1	0.8558	0.8559	0.8527	0.8506
σ experiment set 2	0.8564	0.8571	0.8857	0.8600
σ experiment set 3	0.8568	0.8566	0.8486	0.8480
σ experiment set 4	0.8564	0.8568	0.8528	0.8681

Table 6.3: Posterior b for the aleatory and epistemic case

It can be seen that the means have a higher value than those of the case without aleatory parameters. This makes sense, as b requires a larger shift to let f move in the direction of the data at 0.5.

The spread in calculated means from pMCMC until an MCMC with 1000 samples in the a space is seen to increase. This is logical, as the number of MCMC steps is decreasing from 1E7 to 1E4, implying that the latter will have a larger residual error. However, all experiments have a comparable mean of 0.133, independent of the number of MC steps. Significantly, this appears to suggest that pMCMC is a promising method that is more efficient than MCMC.

6.5 Conclusion

It can be concluded that a MIPR model calibration can be performed for the case of measurement uncertainty only, as well as that of combined measurement and aleatory uncertainty. In the case of only measurement uncertainty, the distributed PI_L posterior of the MIPR model approximates that of the data. For the case where aleatory uncertainty is included as well, the predictions have a larger spread than that of the data.

A pMCMC method is proposed that is significantly more efficient than a MCMC method with explicit aleatory parameter marginalization. Experiments performed on a simple example problem and on the full scale MIPR model calibration suggest that this method gives promising results.

Overall, the results show that a MIPR calibration can be performed. This by itself is not yet sufficient to answer the thesis research question. To determine whether a UQ MIPR model can lead to a step change in completion design, PI_L predictions with these calibrated models must be made for different completion designs. In Chapter 7, it will be

demonstrated if these calibrated models indeed predict the effect of inserting completion skins.

Chapter 7

MIPR Prediction

In Chapter 6, it is shown that a MIPR can be calibrated using fiber optic data. How well this calibrated MIPR can predict changes in completion skin has not yet been tested, this is the objective of this chapter. If predictions of the calibrated MIPR match the response of the truth model, it would indicate that a MIPR can indeed bring about a step change in completion design.

Two types of predictions will be made. The first features a homogeneous completion skin profile, the second a heterogeneous completion skin profile.

7.1 Prediction for a Homogeneous Completion Skin Profile

The homogeneous skin profile that is inserted is given by 7.1

$$s_c = \{2, 2, 2, 2, 2, 2\}. \tag{7.1}$$

The six completion skins are listed from heel to toe. The resulting PI_L prediction is found in Figure 7.1.

The circles indicate the prediction made by the truth model, from which the fiber optic data is distilled. It can be seen that the real change in PI_L falls within the prediction of the calibrated MIPR model. For a homogeneous completion skin change, a calibrated MIPR model can therefore be used as a predictive tool.

7.2 Prediction for a Heterogeneous Completion Skin Profile

In Section 7.1 it is found that a homogeneous skin change can be predicted by a calibrated MIPR model. In some cases, production technologists need to insert a heterogeneous

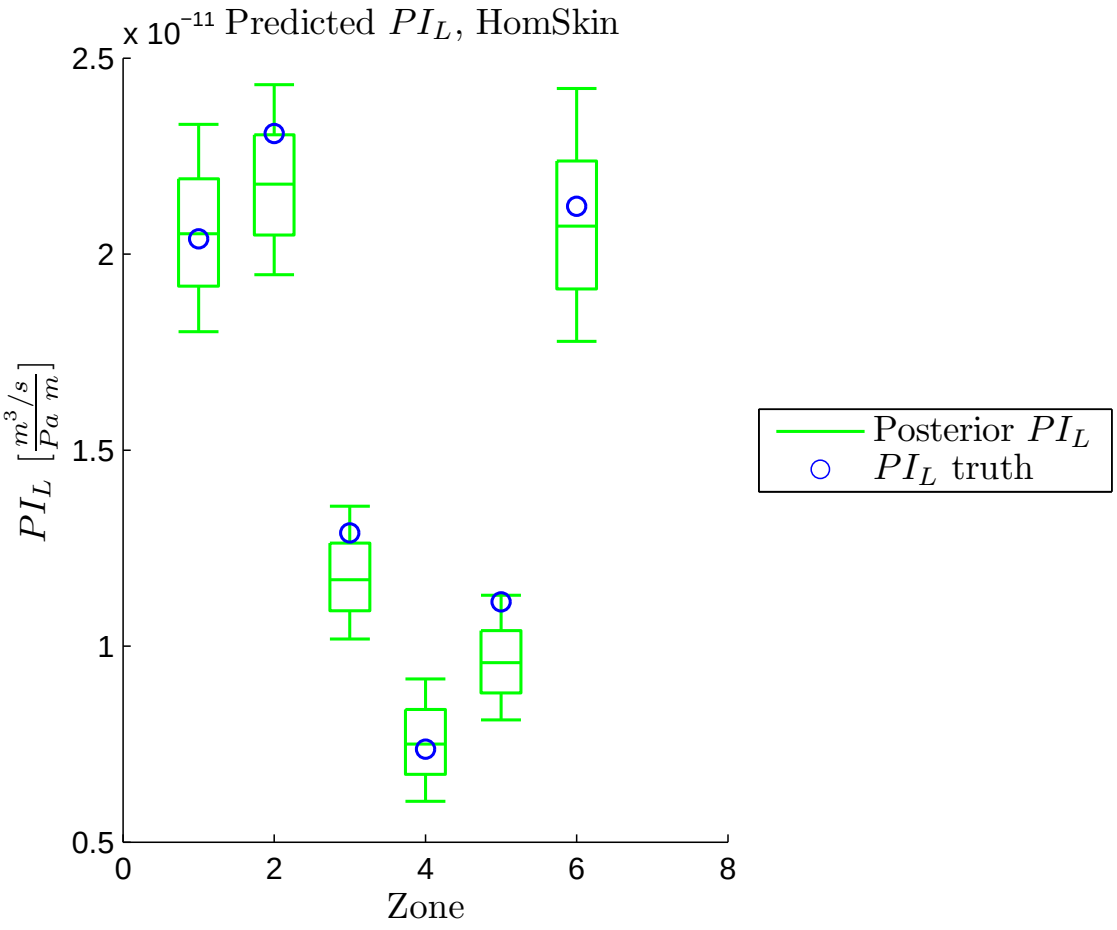

Figure 7.1: PI_L prediction for homogeneous skin with full uncertainty, 2984 samples.

completion skin, for instance if certain zones require different sand inflow treatment than adjacent zones. A heterogeneous completion skin profile tested according to (7.2),

$$s_c = \{1, 3, 1, 3, 1, 3\}. \tag{7.2}$$

The predicted PI_L for this completion skin profile is given in Figure 7.2.

Contrary to the homogeneous skin prediction, the truth lies just outside the outer edges of the uncertainty bounds of the calibrated MIPR prediction. It can be concluded that the calibrated MIPR model cannot predict the change in PI_L for a heterogeneous completion profile. This is because a heterogeneous completion skin profile changes the zone-to-zone flow pattern to which the MIPR model is calibrated. Fluids tend to flow around zones where flow is inhibited, to an adjacent zone. The MIPR does not incorporate these zone-to-zone flows.

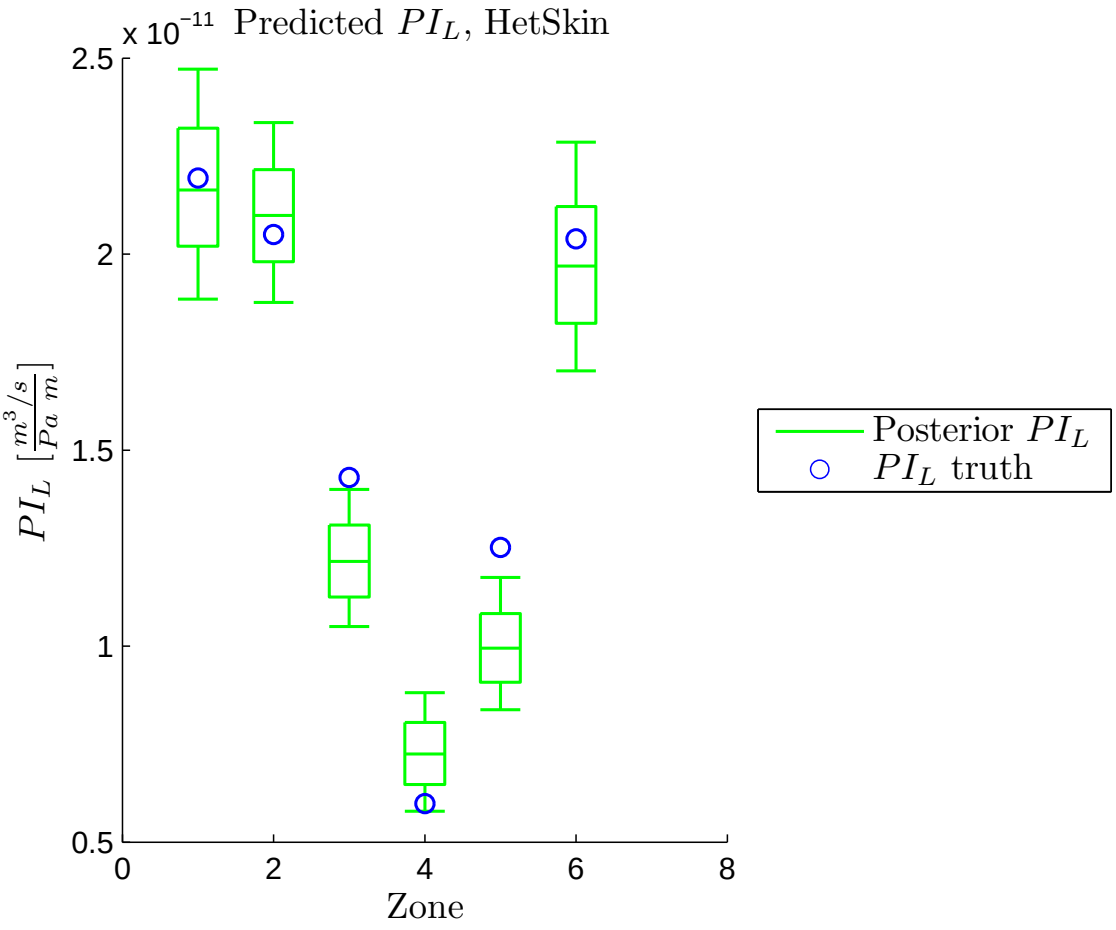

Figure 7.2: PI_L prediction for heterogeneous skin with full uncertainty, 2984 samples.

7.3 Conclusion

It has been found that a MIPR can be calibrated, and can predict PI_L changes for a homogeneous skin profile. However, for a heterogeneous skin profile, the predictions are outside the 10^{th} and 90^{th} percentile, due to changes in zone-to-zone flows in the discretized model. It can still be said that a calibrated MIPR will perform better than an uncalibrated MIPR for predicting heterogeneous skin profiles.

Chapter 8

Conclusions and Recommendations

8.1 Conclusions

The objective of this thesis is to determine if a MIPR using Uncertainty Quantification can lead to a step change in completion design. An answer can be obtained by collecting and analyzing the conclusions from Chapters 4 through 7.

It is found in Chapter 4 that a MIPR can be constructed from several Kuchuk IPR zones coupled with a wellbore network, for an incompressible, isothermal, single phase, pseudo steady flow. The benefit of a MIPR model over a single zone Kuchuk model is that it allows more freedom in the shape of the drainage area, it can handle heterogeneous permeability fields along the direction of the perforation, and it allows a wellbore pressure drop. It is computationally more efficient than a discretized model. The penalty for the increase in functionality of a MIPR model with respect to a Kuchuk model is the insertion of no-flow boundaries between zones.

A verification of the MIPR model has been completed in Chapter 5. For a homogeneous box domain, a single zone Kuchuk IPR model and a MIPR model overpredict the PI by nine and twenty percent respectively, compared to a discretized model. The offset for a Kuchuk zone can be attributed due to compressibility effects, gravity effects, the assumption of an infinitely conductive wellbore and discretization errors in the discretized model. While the MIPR model is composed of Kuchuk IPR models itself, its error is larger. This can be explained by the fact that the zonal average pressures are approximated to be equal to the total average reservoir pressure. Furthermore, MIPR model also assumes radial flow in all intermediate zones; only the two end zones have hemispherical inflow. This implies that a MIPR model is not convergent when the number of zones are increased. The author has used end zones that contain at least twenty percent of the perforation length.
A comparison has also been performed for a domain with a heterogeneous permeability field. It is found that a MIPR model is on the order of twenty times faster than a discretized model. While the MIRP model overpredicts the distributed PI, the shape of the distributions resemble each other. While this means that an uncalibrated MIPR

model should ideally not be used as a completely stand-alone tool, it is concluded that a MIPR model is a candidate for calibration. Potentially, a calibrated MIPR model could lead to a step change in design.

In Chapter 6 a MIPR model is calibrated using fiber optic data distilled from a discretized model. One calibration skin per zone is chosen as epistemic parameter set. Aleatory parameters include the zonal permeability, and, for both the y and z direction, the drainage area size and perforation position. Two techniques are utilized for Bayesian inference, one with an MCMC using an explicit aleatory uncertainty marginalization, and secondly, a proposed 'partitioned MCMC' that the author has not been able to find in literature. In the pMCMC method, aleatory uncertainties become part of the state of the Markov chain. Without an explicit marginalization integral each MCMC step, this method is an order of magnitude faster. It has been found, using both a simple mock experiment and the full scale calibration experiment, that pMCMC gives results comparable to those of the original MCMC method. While these two experiments are not enough to state that the pMCMC method is validated, this method appears very promising to develop further.

The calibrated MIPR predictions for different completion designs are studied in Chapter 7. It is found that the prediction for a homogeneous completion skin equal to two falls within the 10^{th} and 90^{th} percentile. A heterogeneous completion skin, ranging from one to three, results in predictions just outside the 10^{th} and 90^{th} percentile. This can be explained by the fact that the MIPR model has zones that are separated by a no flow boundary. In reality, flow obstruction in one zone will cause increased flow into an adjacent zone. It can be concluded that a calibrated MIPR can predict the effect of a homogeneous completion, and can provide an indication of the effect of a heterogeneous completion.

An answer to the thesis research question can now be given. It is concluded that a MIPR model incorporating UQ can indeed lead to a step change in completion design, if used in conjunction with a discretized model. The strength of next generation reservoir simulators will be in the easy switching between multiple levels of fidelity. A calibrated MIPR can provide a computationally inexpensive tool for preliminary sizing, sensitivity and uncertainty analysis during the initial phases of well development. Using this information, more expensive and rigorous studies can be performed with a discretized model. With this combined approach, more candidate completion designs can be evaluated in a certain period of time, where the selected final designs can be verified with multiple models. Ultimately, with such improvements to the completion design process, another small step can be taken to address the world's energy problem.

8.2 Recommendations

In the process of converging to an outcome of the research question, several areas of follow-up research have been found. These can be split up into model and calibration improvements.

8.2.1 Model Recommendations

Several recommendations can be made to improve the MIPR model. First of all, the proposed condition that an end zone should contain twenty percent of the perforation

length should be investigated in more detail. It is expected that this will be a function of k_x, as well as the skin profile. The easier it is for fluids to flow in the direction parallel to the wellbore, the larger the hemispherical inflow region will be.

Secondly, zonal IPR models with different boundary conditions can be considered. For instance, the influence of aquifers can be included by a specified pressure boundary. Furthermore, research can be performed on an 'inter-zone leakage model'. This would determine the leakage from one zone to another, dependent on the gradient in permeability. The zonal average pressures can then be corrected to some degree even before a calibration is done. The efficiency of a MIPR model can also be compared to that of a discretized model response surface.

Moreover, a recommendation for the discretized model is that the MIPR model user interface could be utilized for the construction of a discretized model as well. This would significantly reduce the setup time during comparison studies. The discretized model itself can also be made more efficient if a better estimate can be given for when the start of pseudo steady flow occurs, so that fewer time steps are required.

8.2.2 Calibration Recommendations

Recommendations have also been found to improve the MIPR calibration. First of all, calibration studies should be performed on the discretized model to further verify the results of the MIPR calibration. It is expected that the discretized model predictions will be accurate even for a heterogeneous skin profile. A discretized model calibration has not been possible within the computational budget of this thesis for the case of a MCMC method with explicit marginalization. The computational cost of this calibration can be reduced significantly by using the pMCMC method.

Furthermore, the UQ techniques used for MIPR calibration can also be generalized to calibrate an entire range of alternative IPR models. Research on UQ calibration could also be interesting to investigate in the domain of well testing, where transient flow is analyzed.

The proposed pMCMC method in this thesis shows promising results. However, the two tests that have been performed are by themselves not sufficient to claim that this is a valid method. Follow up research would be to test the pMCMC method for more complex models and prior distributions types. It is also recommended to pursue a mathematical proof on the equivalence of MCMC and pMCMC posterior distributions.

References

Abdollahzadeh, A., Reynolds, A., Christie, M., Corne, D., Davies, B., & Williams, G. (2011, May). Bayesian optimization algorithm applied to uncertainty quantification. *SPE*.

Adams, S. J. (2005, October). Core to log comparison - what is a good match? *SPE*.

Ahmed, T. (2010). *Reservoir engineering handbook* (4rth ed.). Amsterdam: Elsevier.

AIAA guide for the verification and validation of computer fluid dynamics simulations. (1998). *AIAA Standards*.

Al-Otaibi, A. M., & Ozkan, E. (2005, March). Interpretation of skin effect from pressure transient tests in horizontal wells. *SPE International*.

Andrieu, C., Freitas, N. de, Doucet, A., & Jordan, M. I. (2003). *An introduction to MCMC for machine learning.* Machine Learning, Netherlands.

Ansari, A. M., Sylvester, N. D., Sarica, C., Shoham, O., & Brill, J. P. (1994, May). A comprehensive mechanistic model for upward two-phase flow in wellbores. *SPE Production & Facilities*, pp. 143 – 152.

Beggs, H. D., & Brill, J. P. (1973, May). A study of two-phase flow in inclined pipes. *Journal of Petroleum Technology*, pp. 607 – 617.

Bellarby, J. (2009). *Well completion design.* Amsterdam: Elsevier.

Bond, A., Blount, C., Kragas, T., & Mathias, S. (2004, September). Use of a fiber optic pressure/temperature gouge in an exploration well to minimize formation damage potential and reduce costs during production testing. *Society of Petroleum Engineers*.

Chen, Z. (2007). *Reservoir simulation.* Philadelphia: SIAM.

Dake, L. P. (1978). *Fundamentals of reservoir engineering.* Amsterdam: Elsevier.

Diaconis, P. (2009). *The markov chain monte carlo revolution.* American Mathematical Society, California.

Duns, H. J., & Ros, N. C. J. (1963). vertical flow of gas and liquid mixtures in wells. *Sixth World Petroleum Congress*, *Vol. 22.PD6*.

Economides, M. J., Hill, A., & Ehlig-Economides, C. (1993). *Petrolium production systems.* New Jersey: PTR Prentice Hall.

Fengshu, D., Haolin, C., Jun, L., Chengzhou, N., Gang, C., & Hongxuan, N. (2009). Application of general spatial resolution in seismic survey design. *SEG*, pp. 171 – 175.

Fylling, A. (2002). Quantification of petrophysical uncertainty and its effect on in place volume estimates. *SPE*.

Giger, F., Reiss, L., & Jourdan, A. (1984, September). Reservoir engineering aspects of horizontal drilling. *Society of Petroleum Engineers*.

Gomez, L. E., Shoham, O., Schmidt, Z., Chokshi, R. N., & Northug, T. (2000). Unified mechanistic model for steady-state two-phase flow. *Society of Petroleum Engineers*, *Vol. 5.3*, pp. 339 – 350.

Goode, P. A., & Kuchuk, F. J. (1991, February). Inflow performance of horizontal wells. *SPE Reservoir Engineering*, pp. 319 – 323.

Hagedorn, A. R., & Brown, K. E. (1964, February). The effect of liquid viscosity in two-phase vertical flow. *Journal of Petroleum Technology*.

Hastings, W. K. (1970). Monte Carlo sampling methods using Markov chains and their applications. *Biometrika*, *Vol. 57*, pp. 97–109.

Helman, C. (2011, August 30). Has peak oil come to the non-opec world? Maybe. *Forbes*.

Helton, J., & Davis, F. (2002). *Latin hypercube sampling and the propagation of uncertainty in analysis of complex systems.* Sandia national laboratories, New Mexico.

Hill, A. D., & Zhu, D. (2006, June). The relative importance of wellbore pressure drop and formation damage in horizontal wells. *Society of Petroleum Engineers*.

Hong, T., & Sen, M. K. (2008). Joint Bayesian inversion for reservoir characterization and uncertainty quantification. *SEG*.

Iaccanrino, G., Eldred, M., Doostan, A., & Ghattas, O. (2009). *Introduction to uncertainty quantification.* SIAM CSE Conference, Miami.

Joshi, S. (1988, June). Augmentation of well productivity using slanted and horizontal wells. *AIME*.

Joshi, S. D. (1991). *Horizontal well technology.* Oklahoma: PennWell.

Karcher, B., Giger, F., & Combe, J. (1986, October). Some practical formulas to predict horizontal well behavior. *Society of Petroleum Engineers*.

Kennedy, M. C., & O'Hagan, A. (2000). Predicting the output from a complex computer code when fast approximations are available. *Biometrika*, *Vol. 5.3*.

K.Kragas, Turnbull, B., & Francis, M. J. (2004, May). Permanent fiber optic monitoring at northstar: pressure/temperature system and data overview. *Society of Petroleum Engineers*.

Koelman, J. M. V. A., Lopez, J. L., & Potters, J. H. H. M. (2012, February). Fiber optic technology for reservoirs surveillance. *International petroleum technology conference*.

Koelman, J. M. V. A., & Potters, J. H. H. M. (2012, March). Optical fibers: the neurons for future intelligent wells. *Society of Petroleum Engineers*.

Loeven, G., & Bijl, H. (2008). Probabilistic collocation used in a two-step approach for efficient uncertainty quantification in computational fluid dynamics. *Computer Modeling in Engineering & Sciences*, *Vol.36.3*, pp. 193 – 212.

Lolon, E. P., Archer, R. A., Iik, D., & Blasingame, T. A. (2008, June). New semi-analytical solutions for multilayer reservoirs. *Society of Petroleum Engineers*.

Ma, X., Datta-Gupta, A., & Efendiev, Y. (2008, September). A Multistage MCMC Method with nonparametric error model for efficient uncertainty quantification in history matching. *Society of Petroleum Engineers*.

Maschio, C., Schiozer, D. J., Filho, M. A. B. M., & Becerra, G. G. (2009, September). A methodology to reduce uncertainty constrained to observed data. *Society of Petroleum Engineers*, pp.167 – 180.

Metropolis, N., Rosenbluth, A. W., Rosenbluth, M. N., Teller, A. H., & Teller, E. (1953). Equation of state calculations by fast computing machines. *The Journal of Chemical Physics*, *Vol.21.6*, pp.1087 – 1095.

Nalonnil, A., & Marion, B. (2012, February). High-resolution reservoir monitoring using crosswell seismic. *Society of Petroleum Engineers*, pp.25 – 30.

Novy, R. A. (1995, February). Pressure drops in horizontal wells: when can they be ignored? *SPE Reservoir Engineering*, pp. 29 – 35.

Orkiszewski, J. (1967, June). predicting two-phase pressure drops in vertical pipe. *Journal of Petroleum Technology*, pp. 829 – 838.

Peaceman, D. W. (1977). *Fundamentals of numerical reservoir simulation.* Amsterdam: Elsevier.

Peaceman, D. W. (1978). Interpretation of well-block pressures in numerical reservoir simulation. *Society of Petroleum Engineers Journal*, pp. 183 – 194.

Petalas, N., & Aziz, K. (2000). A mechanistic model for multiphase flow in pipes. *SPE Production Engineering Journal*, *Vol. 39.6*, pp. 43 – 55.

Ryou, S., Frantz, J. H., Holditch, S. A., & Lee, W. J. (1989, September). New, simplified methods for modeling multilayer reservoirs performing at pseudo steady. *Society of Petroleum Engineers*.

Satter, A., Iqbal, G. M., & Buchwalter, J. L. (2008). *Practical enhanced reservoir engineering.* Tulsa: PennWell Corporation.

Schlesinger, S. (1979). Terminology for Model Credibility. *Simulation*, pp. 103 – 104.

Scholtes, S., & Saha, S. (2008, May). Conflicting log and core data: making decisions in deep water GOM. *SPWLA*.

Serag, S., Dernaika, M. R., Hosani, I. A., Hannon, L., Skjaeveland, S. M., & Kalam, M. Z. (2010). Whole core versus plugs: integrating log and core data to decrease uncertainty in petrophysical interpretation and STOIP calculations. *SPE*.

Tailel, Y., & Dukler, A. E. (1976). A model for predicting flow regime transitions in horizontal and near horizontal gas-liquid flow. *AIChE Journal*, *Vol. 22*, pp. 47 – 55.

Tanaka, N. (2010). *World energy outlook 2010.* International Energy Agency, Beijing.

Weinzierl, S. (2000). *Introduction to monte carlo methods.* NIKHEF Theory Group, Amsterdam.

Yudin, E., & Lubnin, A. (2011, October). Simulation of multilayer wells operating. *Society of Petroleum Engineers*.

Appendix A

Theory

A.1 Black Oil Reservoir Simulation

The discretized model used for this thesis uses a black oil fluid, with water, a heavy and a light hydrocarbon component. It can be shown that when this discretized model is solved with a single phase fluid, the governing equations are equal to those solved for Kuchuk IPR, namely (1.4) and (1.5). The black oil equations are written in terms of oil, water and gas (o, w, g) Chen [2007]:

$$\frac{\partial \phi(\rho_w S_w)}{\partial t} = -\nabla \cdot (\rho_w \, \mathbf{u}_w) + q_W, \tag{A.1a}$$

$$\frac{\partial (\phi \rho_{O_o} S_o)}{\partial t} = -\nabla \cdot (\rho_o \, \mathbf{u}_o) + q_O \tag{A.1b}$$

$$\frac{\partial}{\partial t} \left(\phi [\rho_{G_o} S_o + \rho_g S_g] \right) = -\nabla \cdot (\rho_{G_o} \, \mathbf{u}_o + \rho_g \, \mathbf{u}_g) + q_G, \tag{A.1c}$$

where

$$\mathbf{u}_\nu = -\frac{1}{\mu_\nu} \mathbf{k}_\nu \left(\nabla p_\nu - \rho_\nu g \nabla z \right) \qquad \nu = \{o, w, g\}. \tag{A.2}$$

The saturation S is the ratio of the volume occupied by a particular fluid over the total interconnected pore volume. For the closure of (A.1a) through (A.1c), the saturation equation (A.3) and capillary pressures equation (A.4c) are required;

$$S_w + S_o + S_g = 1, \tag{A.3}$$

$$p_{cow} = p_o - p_w, \tag{A.4a}$$
$$p_{cgo} = p_g - p_o, \tag{A.4b}$$
$$p_{cgw} = p_{cow} + p_{cgo}. \tag{A.4c}$$

All the above equations can be reduced to the single phase form of (1.6) . When oil is the only mobile phase, equations (A.3) through (A.4c) become trivial. The same holds for (A.1a), and, if the pressure is above the oil phase bubble point, (A.1c) becomes trivial as well. With the assumption of a horizontal reservoir, this leaves the desired equations (A.1b) and (A.2):

$$\mathbf{u} = \frac{-1}{\mu}\mathbf{k}(\nabla p), \tag{A.5}$$

$$\frac{\partial(\phi\rho)}{\partial t} = -\nabla \cdot (\rho\,\mathbf{u}) + q. \tag{A.6}$$

The representation of the completion in q is calculated with a Peaceman inflow model Peaceman [1977].

The black oil models assume that there are no hydrocarbons dissolved in water, and that there is just a single oil and a single gas phase. For the purposes of investigating a single phase oil flow, the black oil model does not have any limiting assumptions. The dominant source of model error will be that of discretization error.

A.2 Peaceman Inflow Model

Peaceman [1978] was the first to systematically analyze cell to well models, these are still used today. The main problem is that there is a difference between the pressure in the cell that contains the well and the pressure measured in the well itself; the bottom hole flowing pressure. This is because the logarithmic pressure 'cusp' at the wellbore is averaged over the entire cell. Peaceman approached this by finding an equivalent radius r_{eq} at which the pressure equals the steady state bottom hole flowing pressure. Peaceman [1978] investigated several methods to find r_{eq}, one of which was the finite difference approximation where

$$p_1 = p_0 + \frac{q\mu}{2\pi kh}\ln\frac{\Delta x}{r_o}. \tag{A.7}$$

Here p_o is the pressure at the well cell, with p_1 through p_4 being the pressures in the cells adjacent to the well cell edges, forming a symmetric cross. The last term is simply a pressure drop according to a single phase steady radial inflow model. The well is inserted by (A.8)

$$\left(\frac{kh}{\mu}\right)(p_1 + p_2 + p_3 + p_4 - 4p_0) = q. \tag{A.8}$$

Due to symmetry, all the pressures in the cells adjacent to the well cell are equal, therefore combining (A.7) and (A.8) leads to the result of

$$\ln \frac{\Delta x}{r_{eq}} = \frac{\pi}{2}, \tag{A.9}$$

$$r_{eq} = 0.208\Delta x. \tag{A.10}$$

Although the equivalent radius in (A.10) is found to be $0.208\Delta x$, other investigations by Peaceman lead to the conclusion that

$$r_{eq} \approx 0.2\Delta x. \tag{A.11}$$

A.3 Newton–Rhapson Linearization

The different solution techniques use Newton–Raphson methods to solve the nonlinear equations for each time step. The method is described by Chen [2007], starting with (A.12):

$$\mathcal{L}_m[F_m(\mathbf{p}(\mathbf{x}))] = \mathbf{f}_m(\mathbf{x}), \qquad m = 1, 2, \ldots M, \qquad \mathbf{x} \in \boldsymbol{\Omega}. \tag{A.12}$$

Here $\mathcal{L}_m$ is a linear differential operator, F_m is a nonlinear function, $\mathbf{p}$ is a vector of dependent variables, $\mathbf{f}$ is a vector and m the equation number. Using a Taylor series expansion,

$$F_m(\mathbf{p} + \delta\mathbf{p}) = F_m(\mathbf{p}) + \nabla F_m(\mathbf{p}) \cdot \delta\mathbf{p} + \mathcal{O}(|\delta\mathbf{p}|^2). \tag{A.13}$$

Ignoring the last term and substituting back into (A.12) yields

$$\mathcal{L}_m[F_m(\mathbf{p}^l) + \nabla F_m(\mathbf{p}^l) \cdot \delta\mathbf{p}^{l+1}] = \mathbf{f}_m(\mathbf{x}), \qquad m = 1, 2, \ldots M, \qquad \mathbf{x} \in \boldsymbol{\Omega}. \tag{A.14}$$

Here l denotes the number of iterations performed, and $\mathbf{p}^{l+1}$ is the unknown. Then

$$\mathcal{L}_m[\nabla F_m(\mathbf{p}^l) \cdot \delta\mathbf{p}^{l+1}] = \mathbf{g}_m(\mathbf{x}), \qquad m = 1, 2, \ldots M, \qquad \mathbf{x} \in \boldsymbol{\Omega}, \tag{A.15}$$

where $\mathbf{g}_m(\mathbf{x})$ is the residual

$$\mathbf{g}_m(\mathbf{x}) = \mathbf{f}_m(\mathbf{x}) - \mathcal{L}_m[\nabla F_m(\mathbf{p}^l)], \tag{A.16}$$

and $\nabla F_m(\mathbf{p}^l)$ is the Jacobian of F_m. Equation (A.15) can then be solved in terms of the new time step $\delta\mathbf{p}^{l+1}$.

Appendix B

Tables

p $[bar]$	Rs $[scf/stb]$	B_o $[rb/stb]$	μ_o [cP]
1.0300	0.4100	1.0000	7.1160
16.6000	3.9500	1.0560	5.9940
32.1600	8.2800	1.0600	5.0000
40.0000	11.4600	1.0640	4.3380
60.0000	17.8900	1.0780	3.8780
80.0000	24.3200	1.0920	3.4670
100.0000	30.7600	1.1060	3.1000
120.0000	37.1900	1.1200	2.7710
140.0000	43.6200	1.1340	2.4780
150.0000	46.8400	1.1410	2.3430
160.0000	50.0500	1.1480	2.2150
170.0000	53.2700	1.1550	2.0950
180.0000	56.4900	1.1620	1.9810
190.0000	59.7000	1.1690	1.8730
200.0000	62.9200	1.1760	1.7710
210.0000	66.1300	1.1830	1.6740
220.0000	69.3500	1.1900	1.5830
230.0000	72.5700	1.1970	1.4970
234.4600	74.0000	1.2000	1.4600
247.5700	78.2180	1.2090	1.3570
260.6800	82.4340	1.2180	1.2600
273.7800	86.6470	1.2280	1.1710
286.8900	90.8640	1.2370	1.0880
300.0000	95.0800	1.2460	1.0110

Table B.1: PUNQ oil table

$p\ [bar]$	$B_g\ [rb/scf]$	$\mu_g\ [cP]$
1.0300	1.0000	0.0078
16.6000	0.0450	0.0080
32.1600	0.0370	0.0084
40.0000	0.0291	0.0088
60.0000	0.0189	0.0092
80.0000	0.0139	0.0096
100.0000	0.0109	0.0100
120.0000	0.0090	0.0104
140.0000	0.0076	0.0109
150.0000	0.0071	0.0111
160.0000	0.0066	0.0114
170.0000	0.0062	0.0116
180.0000	0.0058	0.0119
190.0000	0.0055	0.0121
200.0000	0.0052	0.0124
210.0000	0.0050	0.0126
220.0000	0.0047	0.0129
230.0000	0.0045	0.0132
234.4600	0.0044	0.0133
247.5700	0.0042	0.0136
260.6800	0.0039	0.0140
273.7800	0.0037	0.0144
286.8900	0.0036	0.0148
300.0000	0.0034	0.0152

Table B.2: PUNQ gas table

Parameter	Description	Value
c_o [1/psi]	Compressibility coefficient	0.0001
c_{vo} [1/psi]	Viscosibility coefficient	0.0
m_o [kg/mol]	Oil molecular mass	0.144
m_g [kg/mol]	Gas molecular mass	0.01
K [Pa]	Bubble point	2.0684

Table B.3: Additional oil parameters

English unit	Conversion factor	SI unit
$[API]$	$141.5/(131.5 + API)$	$[g/cm^3]$
$[BBL]$	$1.589873E-01$	$[m^3]$
$[cp]$	$1.0E-03$	$[Pas]$
$[ft]$	$3.048-01$	$[m]$
$[ft^2]$	$9.290304E-02$	$[m^2]$
$[ft^3]$	$2.831685E-02$	$[m^3]$
$[lbm]$	$4.535924E-01$	$[kg]$
$[md]$	$9.869233E-04$	$[m^2]$
$[psi]$	$6.894757E+09$	$[kPa]$
$[psi]$	$1.450377E-01$	$[kPa]$
$[R]$	$5/9$	$[K]$
$[Btu]$	$\approx$	$[kJ]$

Table B.4: Unit conversion factors Chen [2007]